THE EFFECT OF CARBON ON THE STRENGTH OF THORIUM

by

Robert Lee Skaggs

A Dissertation Submitted to the

Graduate Faculty in Partial Filfillment of

The Requirements for the Degree of

DOCTOR OF PHILOSOPHY

Major Subject: Metallurgy

Approved:

Signature was redacted for privacy.

In Charge of Major Work

Signature was redacted for privacy.

Head of Major Department

Signature was redacted for privacy.

Dean of Graduate College

Iowa State University
Of Science and Technology
Ames, Iowa

1967

TABLE OF CONTENTS

INTRODUCTION

Thorium is the first of the series of elements with partially filled 5f shells. The only naturally occurring isotope, $_{90}Th^{232}$, is radioactive and decays ultimately to the stable $_{82}Pb^{208}$. The crystal structure of thorium below about 1360°C is face centered cubic with a lattice parameter of 5.086Å. Between 1360°C and the melting point at 1750°C, the crystal structure is body centered cubic with a lattice parameter of 4.11Å. The reported physical and thermodynamic properties of thorium have been summarized by Smith (1).

When exposed to a neutron flux, thorium is converted into $_{92}U^{233}$ by the nuclear reaction,

$$\begin{aligned} {}_{90}Th^{232} + {}_{0}n' &\rightarrow {}_{90}Th^{233} + \gamma \\ &\quad\downarrow \\ &\quad {}_{91}Pa^{233} + {}_{-}\beta^{0} \\ &\quad\downarrow \\ &\quad {}_{92}U^{233} + {}_{-}\beta^{0} \ . \end{aligned} \qquad (1)$$

The uranium isotope U^{233} is fissionable and thus, thorium is a source of nuclear fuel. The early studies of the mechanical properties of thorium have been directed toward application in "breeder" type reactors. Work on the mechanical properties of thorium prior to 1956 has been summarized by Milko *et al.* (2). Most of this work was confined to the

measurement of engineering properties at room temperature and above. The findings agree in that all investigators report the flow stress to be a strong function of temperature and carbon content.

Klieveneit (3) studied the flow stress of thorium containing 400 ppm C and 70 ppm N over the range 78°K to 1073°K. The behavior may be divided into three regions: 1) A low temperature range extended from 78°K to about 470°K over which the flow stress showed temperature and strain rate dependence. 2) An intermediate temperature range extended from 470°K to 670°K over which the flow stress showed neither temperature nor strain rate dependence. 3) A high temperature range extended above 670°K where temperature and strain rate dependence were once more observed. A yield point occurred over the low temperature range with the exception of the lowest temperature tested, 78°K. Unlike the sharp yield point observed in steel, the upper yield point occurred only after a plastic strain of 0.005. Further, the flow curve did not fall discontinuously to the lower yield point, but described a smooth minimum before work hardening increased the flow stress. As might be expected in the case of continuous yielding no Luder's bands were observed. Schwope *et al*. (4)

observed a yield point for thorium containing approximately 900 ppm carbon plus nitrogen. The yield point was attributed to the tearing of anchored dislocations away from impurity atmospheres.

The low temperature creep behavior of thorium was studied by Young (5). It was observed that over a limited temperature range, the flow properties of thorium could be described by a function of the form $\dot{\epsilon} = f(\epsilon,\sigma,T,\text{ structure})$. The assumption that (structure) = $f(\epsilon)$ was used to formulate a mechanical equation of state. The material studied was identical to that used by Klieveneit (3) in constant strain rate tensile tests. It was possible to combine tensile and creep data to obtain a flow stress-strain rate relation over a range of strain rate from 10 per second to 10^{-6} per second. Plastic deformation was observed only above a critical stress value. This stress was found to increase with increasing plastic strain but was independent of temperature.

Milko (6) found that the impact behavior of thorium was strongly affected by carbon. Additions of carbon to iodide thorium originally containing 0.02% carbon progressively lowered the impact strength and raised the brittle-ductile transition temperature.

Mickelson and Peterson (7) report the carbon solubility limit in thorium to be 0.35 w/o at room temperature. Thorium appears to be nearly unique among face centered cubic metals in showing this large solid solubility of carbon. Liquid silver, gold, copper, lead, iridium, palladium, and rhodium are reported to reject dissolved carbon as graphite on freezing and to show no measurable solid solubility. Liquid solutions of carbon in aluminum separate into Al_4C_3 and aluminum on freezing. The reported behavior of nickel is conflicting. It appears, however, that solid solubility of carbon in nickel at room temperature is extremely small. In general, the face centered cubic metals show extremely low carbon solubility as summarized by Elliot (8).

Plastic deformation of metal crystals as observed macroscopically results from the movement of dislocations through the lattice. If the flow stress is found to be temperature and strain rate dependent, it can be concluded that dislocation movement is limited by the occurrence of one or more thermally activated processes. The concept of thermally activated plastic deformation assumes that there are obstacles to dislocation movement which are localized in their effect. Such obstacles are defects which are limited

in at least one dimension to several atomic diameters. Because of the localized nature of these defects, random thermal energy fluctuations can assist in overcoming such obstacles to dislocation movement. Micro-processes which are believed to occur due to the combined effect of stress and thermal fluctuations are the following: 1) Non-conservative motion of jogs, 2) Cross-slip of extended dislocations, 3) Overcoming of the elastic interaction between dislocations and impurity atoms, 4) Intersection of forest dislocations, 5) Climb, and 6) Overcoming the Peierls-Nabarro force.

Obstacles to dislocation movement which are large relative to atomic dimensions are not affected by random thermal energy fluctuations. Precipitates, grain boundaries, substructure, and parallel dislocations fall into this category. Although the stress field is believed to fall off rapidly around an incoherent precipitate or a grain boundary, dislocation pile-ups against such obstacles do cause long range stress fields. The observed flow stress, σ, of some solids can logically be divided into two components, the thermally activated stress, σ^*, which is required to overcome short range obstacles, and the athermal stress, σ_μ, which is required to overcome long range obstacles. The thermally

activated component is a function of temperature and strain rate, while the athermal component varies with temperature only through the temperature variation of the elastic constants.

The general expression for plastic deformation of a crystalline solid given by Cottrell (9) is

$$\dot{\gamma} = \rho b \bar{v} \tag{2}$$

where $\dot{\gamma}$ is the rate of shear strain, b is the Burger's vector, ρ is the density of moving dislocations, and $\bar{v}$ is the mean dislocation velocity. The shear strain differs from the normal strain, ϵ, by a constant K_1 so that

$$\dot{\epsilon} = K_1 \rho b \bar{v}. \tag{3}$$

In order to introduce the idea of thermal activation, one may assume that dislocation motion is stepwise, with the dislocation moving a mean distance $\bar{s}$, with a frequency of ν per second. Becker, quoted by Conrad (10), first applied an Arrhenius relation to plastic deformation by assuming that the energy required to overcome an obstacle is a function of stress, and that the solid behaves according to classical Boltzman statistics. The frequency of successful jumps, ν, is given by the expression

$$\nu = \nu^* \exp \frac{-\Delta H(\sigma)}{KT} \tag{4}$$

where ν^* is a frequency related to the DeBye frequency, ΔH is the activation energy and is a function of stress, K is Boltzman's constant, and T is the absolute temperature. By combining Equations 3 and 4, the expression for the strain rate

$$\dot{\varepsilon} = K_1 \rho b \bar{s} \nu^* \exp \frac{\Delta H(\sigma)}{KT} \tag{5}$$

results. By considering both the free energy of plastic deformation and the strain rate to be functions of temperature and stress, Conrad and Wiedersich (11) have developed the expression

$$\Delta H(T,\sigma^*) = -KT^2 \frac{\left[\left(\frac{\partial \sigma}{\partial T}\right)_{\dot{\varepsilon},\varepsilon} - \frac{\sigma}{\mu} \frac{d\mu}{dT} \right]}{\left(\frac{\partial \sigma}{\partial \ln \dot{\varepsilon}}\right)_{T,\varepsilon}} \tag{6}$$

for the activation energy of deformation in terms of quantities measurable in a tensile test, where μ is the shear modulus, and the other terms have been defined previously.

Schoeck (12) has criticized expression (6) on the ground that it neglects a configurational entropy term. Although the criticism appears to be valid, Schoeck's corrected expression for activation free energy is cumbersome to use and yields a result substantially the same as (6). An expression for activation volume, V^*, which is a measure

of the volume over which the micro-process occurred, has been shown by Conrad (13) to be

$$v^* = -KT \left(\frac{\partial \ln \dot{\epsilon}}{\partial \tau} \right)_{T,\epsilon} \qquad (7)$$

The measurement of activation energy and activation volume has been used to study plastic deformation in both the body centered cubic and the closest packed structures. The theory and experimental procedures are discussed by a number of authors: Conrad (10), Gregory (14), Mordike and Haasen (15), Basinski (16) and Schoeck (12).

Investigators have noted striking differences between the mechanical behavior of body centered cubic metals and that of face centered cubic metals. Conrad (13) has summarized much of the work on the temperature and strain rate dependence of yield stress in body centered cubic metals. The yield strength of the body centered cubic metals increases steeply at low temperature while the strength of the face centered cubic metals varies only slightly from room temperature to absolute zero. Further, the strain rate parameter, $(\Delta\sigma/\Delta \ln \dot{\epsilon})_{\epsilon,T}$, increases to a maximum and then decreases over a broad temperature range in the case of the body centered cubic metals, but remains small and is nearly

constant with temperature for the face centered cubic metals. Wessel (17) has emphasized the difference between the strong temperature dependence of strength observed in body centered cubic metals and the weak dependence observed for the closest packed structures. Understandably, much effort has been devoted to rationalizing the differences in behavior in terms of structure.

Fleischer (18) has proposed a strengthening mechanism based on the elastic interaction between moving dislocations and defects. Cochardt et al. (19) have calculated the elastic interaction U_{DC} by the expression

$$U_{DC} = -\sigma_{ik}\epsilon_{ik}a^3 \qquad (8)$$

where U_{DC} is the interaction energy, σ_{ik} is the dislocation stress tensor, ϵ_{ik} is the defect strain tensor, and a is the lattice parameter. They have shown that the elastic interaction given by expression (8) is important for screw as well as edge components if the defect is assumed to produce a non-spherical distortion. In summarizing the results of screw dislocation-defect interactions, Fleischer (20) has emphasized that in either the body centered cubic or the face centered cubic lattice, the interaction energy is proportional to $(\epsilon_1 - \epsilon_2)$, the tetragonality of the strain caused by

the impurity. It is believed that interstitial impurities in body centered cubic metals are located in the octahedral holes, as shown by Williamson and Smallman (21). The six atoms surrounding this hole are not symmetrically distributed, and the distortion produced by an impurity is non-spherical. On the other hand, six atoms are symmetrically placed around the octahedral holes in the face centered cubic cell, and the distortion is assumed to be spherical. Hence, according to this analysis, both screw and edge components interact elastically with interstitial impurities dissolved in the body centered cubic lattice, while only the edge component does so in the face centered cubic lattice.

Bechtold (22) has rationalized the difference between the temperature dependence of the flow strength of body centered cubic and face centered cubic metals on the basis of the symmetry of interstitial positions. This view, however, is not universally accepted. A number of mechanisms have been proposed whereby interstitial atoms might interact strongly with a screw dislocation. Seeger et al. (23) have proposed a process involving mutual relaxation of an interstitial atom from a normal octahedral site and a host atom from a face centered cubic corner site to form a configura-

tion with tetragonal symmetry. Van Bueren (24) has pointed out that in closest packed structures the dislocations are extended so that at least one of the resulting partials must have some edge character.

Another source of resistance to a moving dislocation is the Peierls-Nabarro force, often termed lattice friction. The elastic continum model of a solid is not valid in the immediate vicinity of a dislocation. In moving, a dislocation alters locally the number of atom nearest neighbors, and doing so, experiences a drag force. Based on a simple two dimensional solid, the Peierls-Nabarro force is given by the expression

$$f = \frac{2\bar{\mu}}{(1-\nu)} \exp \frac{-2\pi a}{b(1-\nu)} \qquad (9)$$

where μ is the shear modulus,

b is the Burger's vector,

ν is the Poisson's ratio, and

a is the interplanar separation.

The ratio a/b is greater for the face centered cubic system than it is for the body centered cubic system. It follows that the force calculated by expression 9 will be greater for body centered cubic metals than for face centered cubic metals. The Peierls-Nabarro force is short range in nature,

and so, thermal fluctuations can assist in overcoming it. Conrad (13) has reviewed the data on body centered cubic metals and has concluded that the temperature and strain rate dependence of the flow stress is due to Peierls-Nabarro resistance to dislocation motion. This conclusion was based on the fact that the experimentally determined values of activation energy and of activation volume were independent of structure, impurity content, strain, and method of determination.

Study of the metals with closest packing has not, in general, shown the strong temperature dependence of flow stress observed in the body centered cubic metals. Wessel (17) observed that the proportional limit of commercially pure nickel doubled in going from 600°K to 4.2°K, and that crystal bar zirconium behaved similarly. Mild steel, tantalum, and molybdenum showed six to eight fold increases over the range 600°K to 78°K.

Geil and Carwile (25) measured the mechanical properties of high purity nickel and of high purity copper over the temperature range 78°K to 373°K. It was found that in each case the proportional limit was essentially constant over the entire range. At higher strains, the flow stress showed

moderate temperature dependence. Thus, the flow stress of a strained face centered cubic polycrystal, even of high purity, has a thermally activated component. A number of mechanisms responsible for temperature and strain rate dependence in strained face centered cubic polycrystals are recognized. Seeger (26) has summarized the processes leading to the temperature and strain rate dependence of flow stress in face centered cubic metals. All of these processes are strain dependent since they are affected by the dislocation density.

Although much early work indicated that closest packed structures did not show strong temperature and strain rate dependence, there is evidence that this is not always true. In several cases, large temperature and strain rate dependence of flow stress have been noted in hexagonal close packed metals containing interstitial impurities. The work on polycrystalline titanium has been summarized by Orava et al. (27). Weinstein (28) has studied polycrystalline zirconium of commercial purity. Examples of interstitial strengthening of face centered cubic metals and alloys are less abundant. Flinn (29) prepared solid solutions of 0.5 and 1 atomic percent carbon in nickel by quenching specimens from

an elevated temperature. The proportional limits of the resulting solid solutions were higher than that of pure nickel, and a sharp increase in strength was observed with decreasing temperature. The proportional limit of the 0.5% C alloy rose from 10,000 psi at 373°K to 38,000 psi at 4.2°K. Because the alloy was super-saturated, there is reason to suspect that the strengthening could be due to effects other than simple solution hardening. Sonon and Smith (30) report that the yield strength and yield strength variation with temperature of type 330 austenitic stainless steel increased with total interstitial impurities. The configuration of dislocation arrays observed after deformation led them to suggest that short range ordering had occurred.

Boniszewski and Smith (31) have cathodically charged nickel with hydrogen in concentrations up to 4 atom percent. Although the ductility of the nickel was drastically lowered by hydrogen, no large changes in strength or strength variation with temperature and strain rate were observed.

Thorium differs from the other face centered cubic metals in that the yield strength increases rapidly at low temperature. In this regard, the mechanical properties of thorium resemble more closely those of the body centered cubic

metals. Thorium also differs from the face centered cubic metals which have been more extensively studied, such as copper and aluminum, in that is shows a relatively high carbon solubility. Carbon is known to significantly increase the hardness and strength of thorium. Consequently, it was believed that the systematic study of the effect of carbon content, temperature, and strain rate upon the strength and yield point behavior of thorium would represent a tangible contribution to the understanding of alloy hardening. Since the thermal component of flow stress is a function of temperature and strain rate, it should fall to zero at high temperature and low strain rate. In principle, it is possible to measure the athermal component directly at room temperature and below by reducing the strain rate to a value approaching zero. The direct measurement of the athermal component of flow stress together with its study as a function of carbon content was also an objective of this work.

EXPERIMENTAL PROCEDURE

Specimen Preparation

The thorium used in this investigation was produced by reduction of thorium tetrachloride with excess magnesium to form a low melting intermediate alloy from which thorium sponge is obtained by heating under vacuum. This method has been described by Peterson *et al.* (32). In order to eliminate scatter caused by composition variations, most of the specimens used in this investigation were prepared from thorium from one reduction. A second batch was used to prepare the highest carbon concentration specimens. The effect of carbon was so pronounced at this concentration that the small composition difference between the two batches prior to alloying was unimportant. Chemical analyses of the two lots after arc melting and electron beam melting are given in Table 1. In order to obtain homogeneity in the base metal, the electron beam melted ingot was rolled to 1/4 inch thick plate and sheared into 1/2 inch square pieces. Alloys were prepared by arc-melting the thorium with a weighed amount of carbon in the form of high purity spectrographic graphite electrodes. The buttons were melted and turned five times to assure uniform carbon distribution. The alloys were

then melted into elongated molds approximately 6 inches long by about 3/4 inch diameter. These arc-melted rods were subsequently rolled and swaged to 3/8 inch diameter.

Specimens used in the constant stress tests were machined from the as-swaged 3/8 inch rod. The specimen was 2½ inches overall in length, was threaded for a length of 0.4 inch on each end with 3/8-16 National coarse thread, and had a reduced gage length 1.6 inches in length and 0.252 ± 0.001 inch in diameter. A 1/8 inch radius transition section was used between the gage length and the thread.

Tensile specimens were prepared by swaging annealed 3/8 inch diameter rod to 0.102 ± .001 inch in 5 passes. The as-swaged wire was cut to lengths of 2 inches, annealed, and the center 1 inch gage length electropolished to 0.100 ± .001 inch. Electropolishing was done in a methyl alcohol-6% perchloric acid electrolyte at -70°C and using a D.C. potential of about 30 volts. In testing, the specimens were gripped for a length of 1/2 inch at each end by a serrated four jaw collet, which in turn, was secured by a tapered compression nut. This arrangement was satisfactory in that no slipping occurred in the grips and negligible deformation was observed outside the ungripped 1 inch gage length. Because

of the ductility of thorium, the sharp notches caused by the serrated grips posed no problem.

Both the creep and tensile specimens were annealed for one hour at 730°C. The resulting structures consisted of equi-axed recrystallized grains with a grain size of approximately 3200 grains per square millimeter for the tensile specimens and 2200 grains per square millimeter for the creep specimens. The finer grain size of the tensile specimens was due to the larger amount of cold work that material received prior to recrystallization. Preliminary work indicated that the grain size strongly influenced the yield point behavior of thorium, but had little effect on the flow stress beyond two percent strain. The highest purity material, which contained less than 4 ppm carbon, was prepared by an electrotransport technique described by Peterson et al. (33). After the specimens had been prepared, a sample from each alloy composition was analyzed for carbon, nitrogen, oxygen, and hydrogen. The results of these analyses are given in Table 2.

Constant Strain Rate Measurements

The tensile machine used in this investigation was a screw-driven, Riehle Model FS-10 Universal Screw Power Testing Machine. The cross-head speed range of this unit is from

0.002 to 2.0 inches per minute. The actual cross head speed was found to differ from the value indicated on the selection dial by less than ± 10%. Calibration performed by the Budd Company showed the load measurement to be correct to within ± 1% on all scales.

Measurements were done with the specimen maintained at constant temperature by immersion in various baths. With the exception of two temperatures, constant freezing or boiling media, as described by Mordike and Haasen (34), were used. At 150°C, silicone oil heated by an immersion heating coil was used. The measurements at 300°C were done in air using a cylindrical resistance furnace. In these cases, a chromel-alumel thermocouple, held directly against the tensile specimen by wrapping with tantalum foil, was used to actuate a temperature controller.

A Polyanyi-type cage to which the specimen was attached extended below the cross head as shown in Figure 1. The entire cage was immersed in the various media for temperature control. The upper end of the specimen was attached to a pull rod, and in this way was placed in tension by downward movement of the cross head.

Modifications of the basic testing arrangement were re-

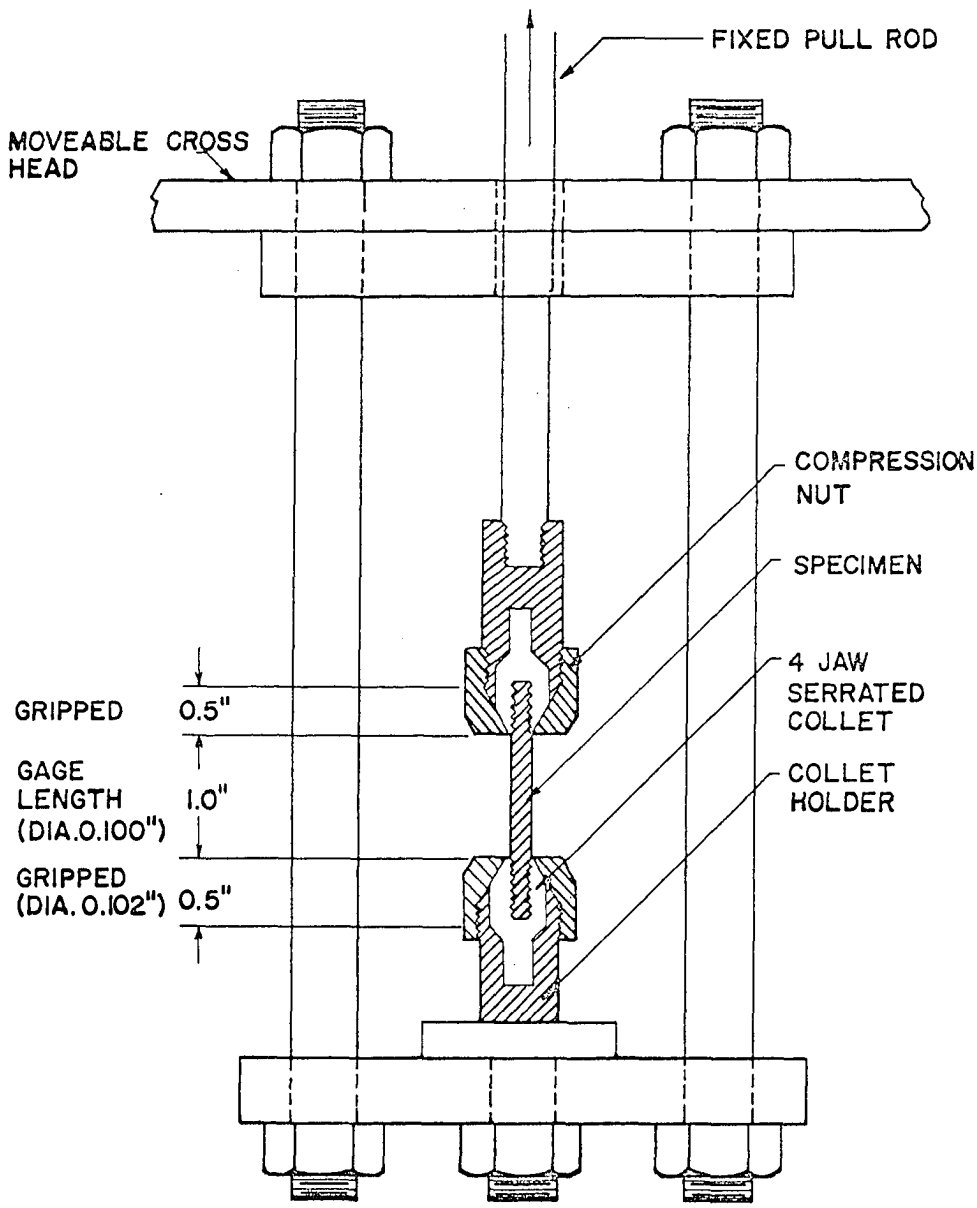

Figure 1. Schematic view of loading and gripping arrangement used in constant strain rate tensile tests

quired for testing in liquid helium. A double Dewar cryostat together with an elongated compression tube of the type described by Haasen (35) was used. A smaller specimen, 0.070 inch diameter, was used for the liquid helium testing. This reduced the loads encountered during testing and allowed the use of a compression tube 26 inches long, 1¼ inch in diameter, and 0.020 inch in wall thickness. The design used was adequate mechanically and limited heat transfer down the tube so that the helium boil off rate was not excessive.

Since the samples were immersed in various baths, it was necessary to measure the elongation indirectly by measuring the cross head motion of the test machine with a Riehle Model DC Deflectometer. This device transmits vertical motion through a lever system to actuate a differential transformer. Magnification of X20 was used for the bulk of the tensile testing although higher values, up to X200, were used in the yield point studies. The cross-head motion signal and the load signal were recorded by a Riehle Model RD-5 Recorder which traced the load-elongation plot. True stress-strain curves were derived from load-elongation traces by a technique based on the assumption that the specimen and machine behave as two elastic members in series. In the elastic

range, the total cross head motion, ΔL, is given by the expression

$$\Delta L = \Delta l_m + \Delta l_E \tag{10}$$

where Δl_m is the elastic deformation of the machine, and Δl_E is the elastic elongation of the specimen. After yielding occurs,

$$\Delta L = \Delta l_m + \Delta l_E + \Delta l_p \tag{11}$$

where Δl_p is the plastic elongation of the specimen. It is assumed that the elastic force constants K_m for the machine and K_E for the specimen do not vary with either load or elongation. In both the elastic and plastic region, the total load, P, is given by the expression

$$P = K_m \Delta l_m. \tag{12}$$

In addition,

$$P = K_E \Delta l_E. \tag{13}$$

The plastic elongation of the specimen is then

$$\Delta l_p = \Delta L - P\left(\frac{K_E + K_m}{K_m K_E}\right) \tag{14}$$

The plastic strain is given by the expression

$$e_p = \frac{\Delta l_p}{l_o} \tag{15}$$

where e_p is the plastic unit strain, and l_o is the original

specimen length. The relation between engineering stress and true stress σ is given by Dieter (36) as

$$\sigma = P/A_o(1+e_p) \tag{16}$$

where A_o is the original specimen cross sectional area. Similarly, the true plastic strain e_p is given by

$$\epsilon_p = \ln(1+e_p). \tag{17}$$

In practice, increments of true strain are chosen, and the corresponding values of Δl_p were laid off along the X axis of the load-elongation plot. The intersection of the load elongation plot with lines of slope K_E+K_M/K_MK_E gives the load P at strain $\ln(1+e_p)$. The product $P/A_o(1+e_p)$ gives the corresponding true stress.

Two specimens were tested at each temperature and the cross head travel speed changed cyclically by a factor of 20 during each test. Cross head speeds corresponded to nominal strain rates of 3.3×10^{-5} per second and 6.67×10^{-4} per second in the low range and 6.67×10^{-4} per second and 1.33×10^{-2} per second in the high range. Strain rate changes were made at intervals of from 0.01 to 0.05 inches elongation. A discontinuous load elongation trace resulted, and it was necessary to interpolate in order to construct constant strain rate

true stress-true strain curves. This practice was justified by the fact that interpolated curves for a strain rate of 6.67×10^{-4} per second were essentially the same whether derived from high range or low range data.

Constant Stress Tests

In order to extend the measurement of flow stress to strain rates below those obtainable with a tensile test machine, it was necessary to use a constant stress or "creep" test. Measurement of flow stress at constant stress was made by using balanced arm, dead weight loading systems. The machines were modified to allow the use of a constant temperature bath. This was accomplished with an arrangement similar to that used in the constant strain rate tests by attaching the specimen inside a compression load tube which extended below the rigid cross head of the creep machine.

Elongation was measured with bonded strain gages, type HE-181-B, manufactured by the Budd Company, Instruments Division. Changes in the resistance of the gage resulting from strain were measured using a Wheatstone type balancing bridge, Baldwin Lima Hamilton Model 20. The theory and practice of electrical resistance strain measurement have

been treated by Perry (37). In order to compensate for changes in specimen length due to temperature variations, a "dummy" gage was attached to an unstressed specimen and was included in the Wheatstone bridge circuit. Since the coefficient of thermal expansion for thorium is about 11×10^{-6} per ^{o}C, it was desirable to limit the temperature difference between the active and the compensating strain gage to about $0.1^{o}C$. At $273^{o}K$, the specimens were immersed in an ice-water mixture in Dewar flasks. At $300^{o}K$ the temperature of the mineral oil bath was controlled by a mercury thermometer switch, "Microset" Model C-18783, manufactured by the Precision Scientific Company.

Considerable attention was paid to assuring the mechanical and electrical integrity of the bonded resistance strain gages. The bond between the specimen and the strain gage epoxy backing film was made using Budd GA-4 cement, an unfilled heat cured epoxy cement. The best results in attaching the strain gages were obtained by following the manufacturer's instructions (38). After the cement had been cured and the lead wire connections had been soldered, the bonded gages were visually inspected for defects at X10 with a binocular microscope. The gage was then tested electric-

ally by measuring the resistance of the gage itself and the gage to specimen resistance. Gages were not used if the resistance fell outside the manufacturer's specification, 120 $\pm$ .05 ohms. Those deviations found were always on the high side of the acceptable range and could be associated with damage which occurred during attachment. Low gage to specimen resistance caused by dirt and moisture on the gage surface resulted in erratic resistance readings during subsequent use. The resistance was increased to values of greater than 20×10^6 ohms by cleaning the specimen in acetone and heating at 100°C immediately before the application of the nitrile rubber Budd GW-2 waterproofing compound. Further checks on the condition of the gage and bond were performed during the course of each creep test. Since the modulus of thorium is known, each load change allows a check on the gage attachment, the electrical circuit, and the loading system.

The critical stress, σ_C, is defined as the minimum stress to produce a measurable plastic strain rate. In principle, this quantity could be measured by the addition of load in small increments until plastic deformation was observed. Thorium undergoes anelastic deformation on loading and unloading which complicates the determination of σ_C by

the above straightforward approach. The method used in this investigation was to estimate the critical stress, and to apply a stress σ_1, which was greater by, perhaps, 2000 psi. After the initial creep rate of about $1x10^{-9}$ per second had been measured at σ_1, the stress was reduced to a value large enough to maintain alignment of the specimen. A second stress σ_2, smaller than σ_1, was then applied immediately and the initial creep rate once more observed. This process was repeated until a stress was reached where no additional deformation was observed during a 60 hour period. This stress was defined as the critical stress. Once the critical stress had been established, strain rates greater than $1x10^{-9}$ at successively higher stress levels were obtained by measuring the time for plastic deformation of from 10 to $200x10^{-6}$ to occur depending on the rate. This technique was usable to strain rates of $1x10^{-6}$ per second, or just below the lower range obtained in tensile tests. Creep and tensile test data were thus combined to establish a flow stress-strain rate relation over the range from 10^{-12} to 10^{-2} per second at a given temperature and strain. Since the entire "creep" portion of the curve is obtained using one specimen, the effect of the $1000\text{-}2000x10^{-6}$ plastic strain which occurred during

the creep testing must be evaluated. In several cases it was necessary to repeat the procedure described above using the same specimen. It was found that the entire flow stress-strain rate curve below strain rates of 1×10^{-7} per second could be reproduced to within 500 psi using previously strained specimens. This practice was possible because the rate of work hardening of thorium is low and the total strain which occurred during the measurements was small. The rate of work hardening for thorium at $273^{\circ}K$ is about 1×10^{5} psi per unit strain. As a result of 2000×10^{-6} plastic strain, an increase in flow stress of about 100 psi is expected. Thus, the measurements can be considered to be at constant strain.

Table 1. Analysis of electron beam melted thorium ingots

	Ingot one	Ingot two
C	112 ppm	154 ppm
N	48	52
O	84	127
Al	~20	~20
Ca	<20	<30
Cr	<20	<20
Fe	<20	<20
Mg	<20	<20
Mn	<20	<20
Ni	<20	<20
Si	<20	<20
Ti	N.D.	N.D.
Y	N.D.	N.D.
Ta	N.D.	N.D.
W	N.D.	N.D.

Table 2. Analysis of thorium-carbon alloy specimens after fabrication and annealing

Carbon content	O	N	H
100 ppm	208 ppm	34 ppm	2 ppm
200	169	25	2
400	98	22	8
1000	169	24	N.D.
1500	202	N.D.	N.D.

RESULTS

The strength of thorium was found to be a function of the carbon content, temperature, strain, and strain rate. For a given alloy composition, strain, and strain rate, the flow stress decreased linearly with temperature from absolute zero to 300°K and then approaches asymtotically a nearly temperature independent value at approximately 550°K. The flow stress above 550°K is a function of carbon content and strain, but not of strain rate. At temperatures below 550°K, the flow stress increases with increasing carbon content, strain, and strain rate. The variation of the 0.1% offset strength with temperature for each of the carbon contents is shown in Figure 2. Similar plots of flow stress at 2 percent and 15 percent true strain are shown in Figures 3 and 4, respectively. It appears that the flow stress is the sum of an athermal component, σ_μ, and a thermally activated component, σ^*. The magnitude of σ^* is a function of the carbon content, temperature, and strain rate, but is almost independent of strain. The athermal component is a function of carbon content and strain, but is independent of strain rate, and nearly inde-

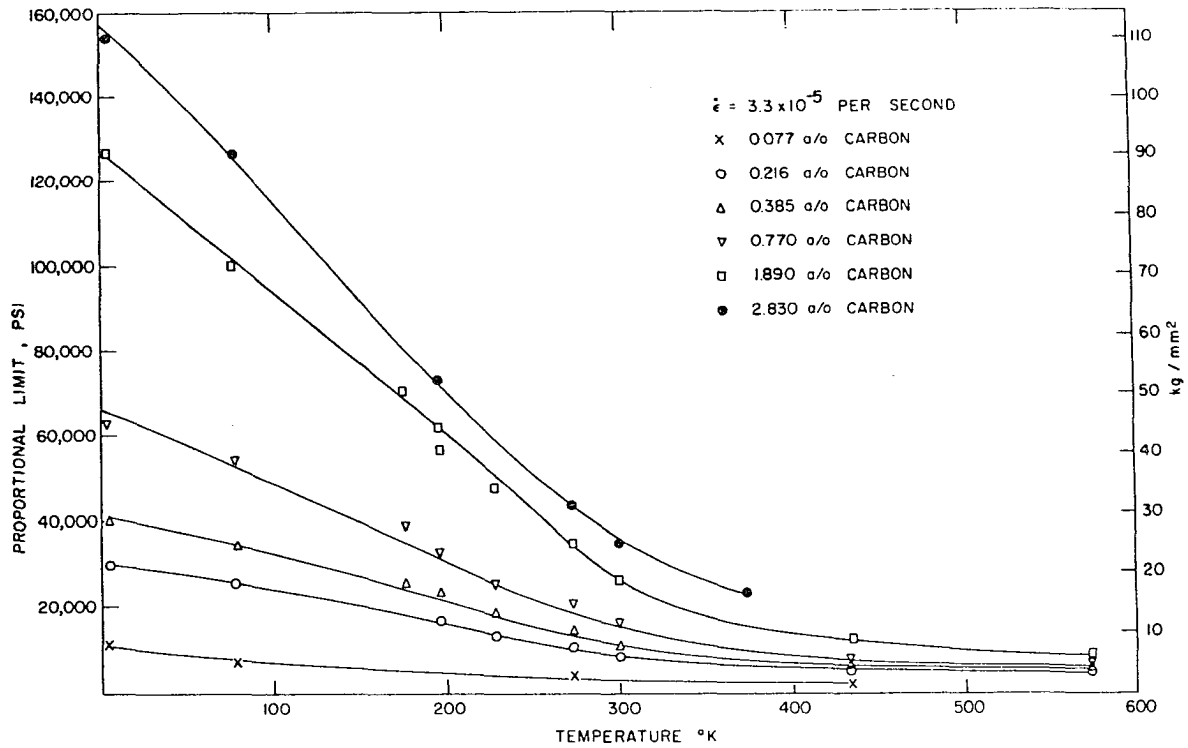

Figure 2. Variation of the 0.1 percent offset flow stress with temperature for a series of thorium carbon alloys

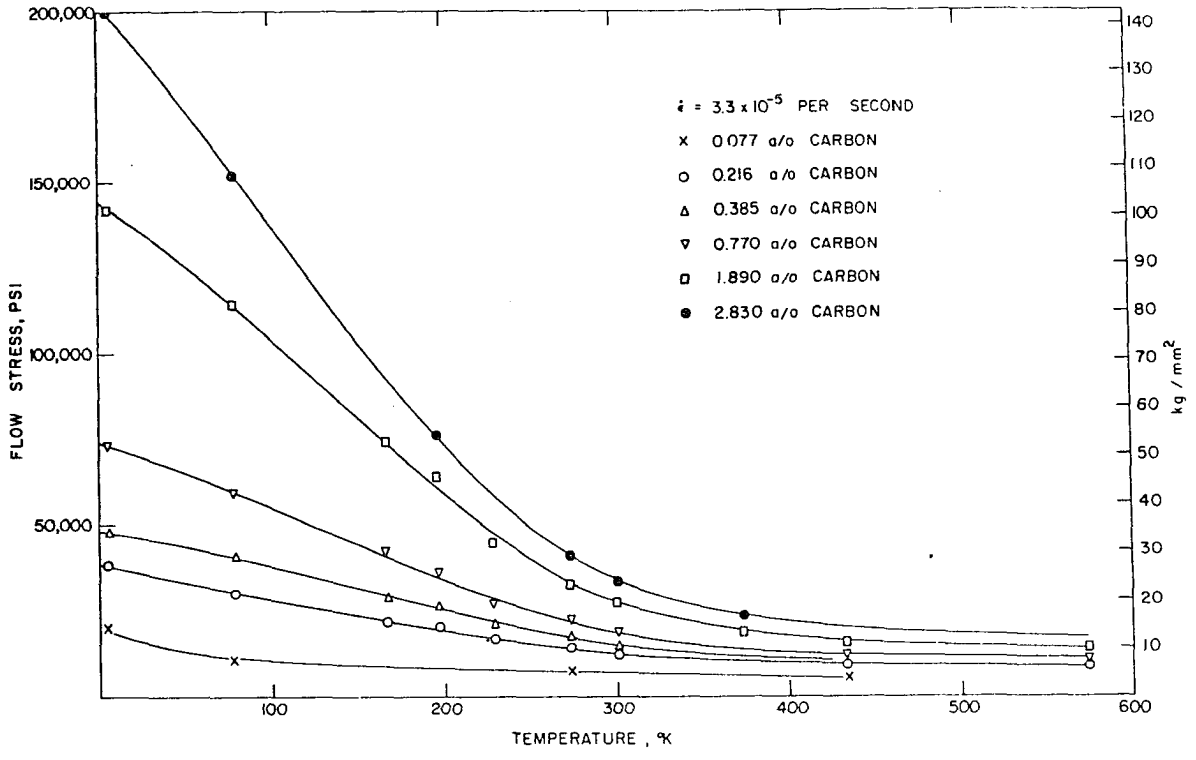

Figure 3. Variation of the 2 percent offset flow stress with temperature for a series of thorium-carbon alloys

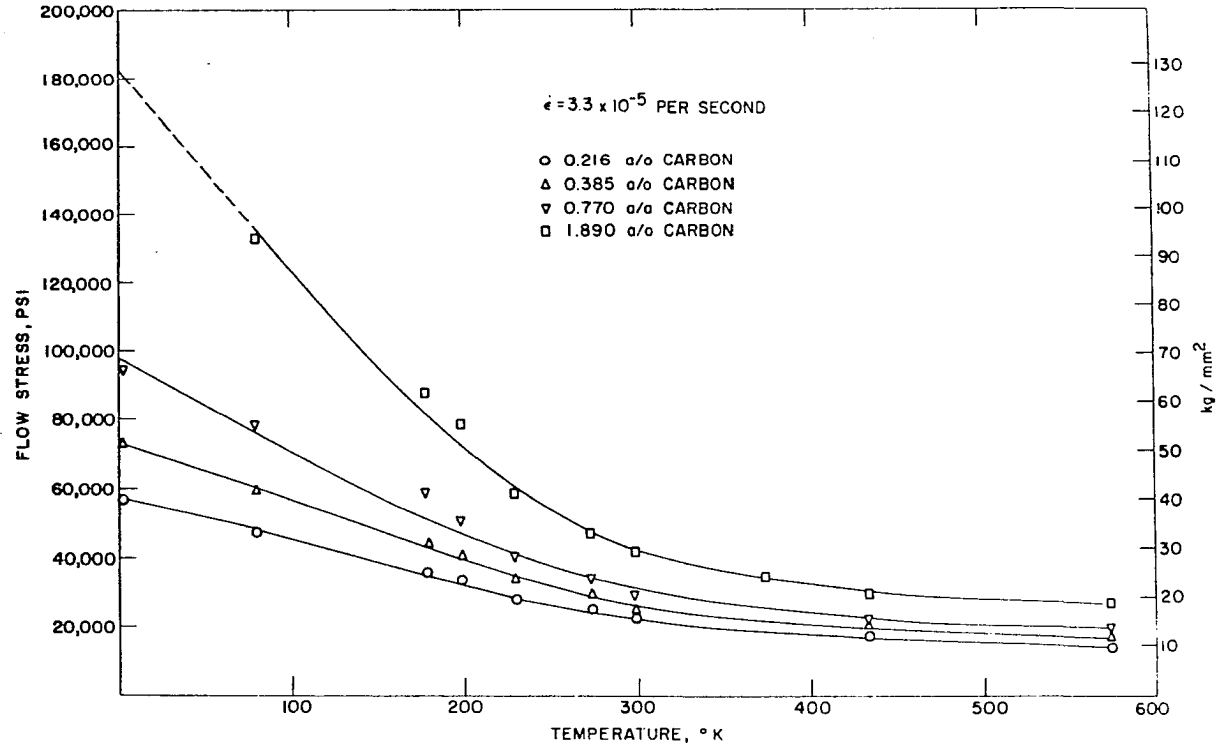

Figure 4. Variation of the 15 percent offset flow stress with temperature for a series of thorium carbon alloys

pendent of temperature. These relations are summarized as

$$\sigma = \sigma^* fn(C_{eff}, \dot{\varepsilon}, T) + \sigma_\mu fn(C_{eff}, \varepsilon) \qquad (18)$$

where C_{eff} is the effective carbon content, ε is the strain, $\dot{\varepsilon}$ is the strain rate, and T is the absolute temperature. In order to obtain σ^* from a plot of flow stress as a function of temperature, the method of Seeger as described by Conrad and Wiedersich (11) was used. The temperature and strain rate independent flow stress at 550°K was taken to be the athermal component. In order to estimate the athermal component at any temperature the high temperature portion of each of the flow stress curves was extrapolated to 0°K with a slope equal to the variation of the elastic constants with temperature. This slope, $d\sigma_\mu/dT$, was estimated to be 3.6 psi/°K from the elastic constants for thorium reported by Armstrong et al. (39).

The athermal component was also measured directly by relaxation experiments and by constant stress measurements. Stress relaxation experiments were conducted in a tensile test machine at 433°K. The cross head movement was stopped at several intervals during a tensile test, and the decrease in load as a function of time observed. After 5 minutes a constant load was reached. The average strain rate during

the relaxation period was calculated assuming that the machine was perfectly rigid. The expression for the average strain rate ($d\epsilon/dt$), was

$$(d\epsilon/dt) = \Delta\sigma/E\Delta t \qquad (19)$$

where $\Delta\sigma$ is the decrease in stress, E is Young's modulus for thorium, and Δt is the time interval. The resulting strain rates were $1x10^{-6}$ per second or less. In this way the stress-strain curve was estimated to $1x10^{-6}$ per second for each of the thorium carbon alloys.

Constant stress measurements were made on the alloys at 273°K and 300°K. It was found that for each sample there was a stress below which plastic strain did not occur at a measurable rate. This critical stress was a function of composition and strain, but not of temperature over the range from 273°K to 300°K. For a given carbon content and strain, the critical stress measured at 273°K and 300°K by the constant load technique, the flow stress at 433°K measured by the relaxation technique, and the strain rate independent flow stress at 573°K were all equal to within the accuracy of the measurements. The values of the critical stress measured at 273°K and 300°K with zero prestrain are shown in Table 3 for alloys containing 0.216, 0.385, 0.770, and 1.89 atom percent

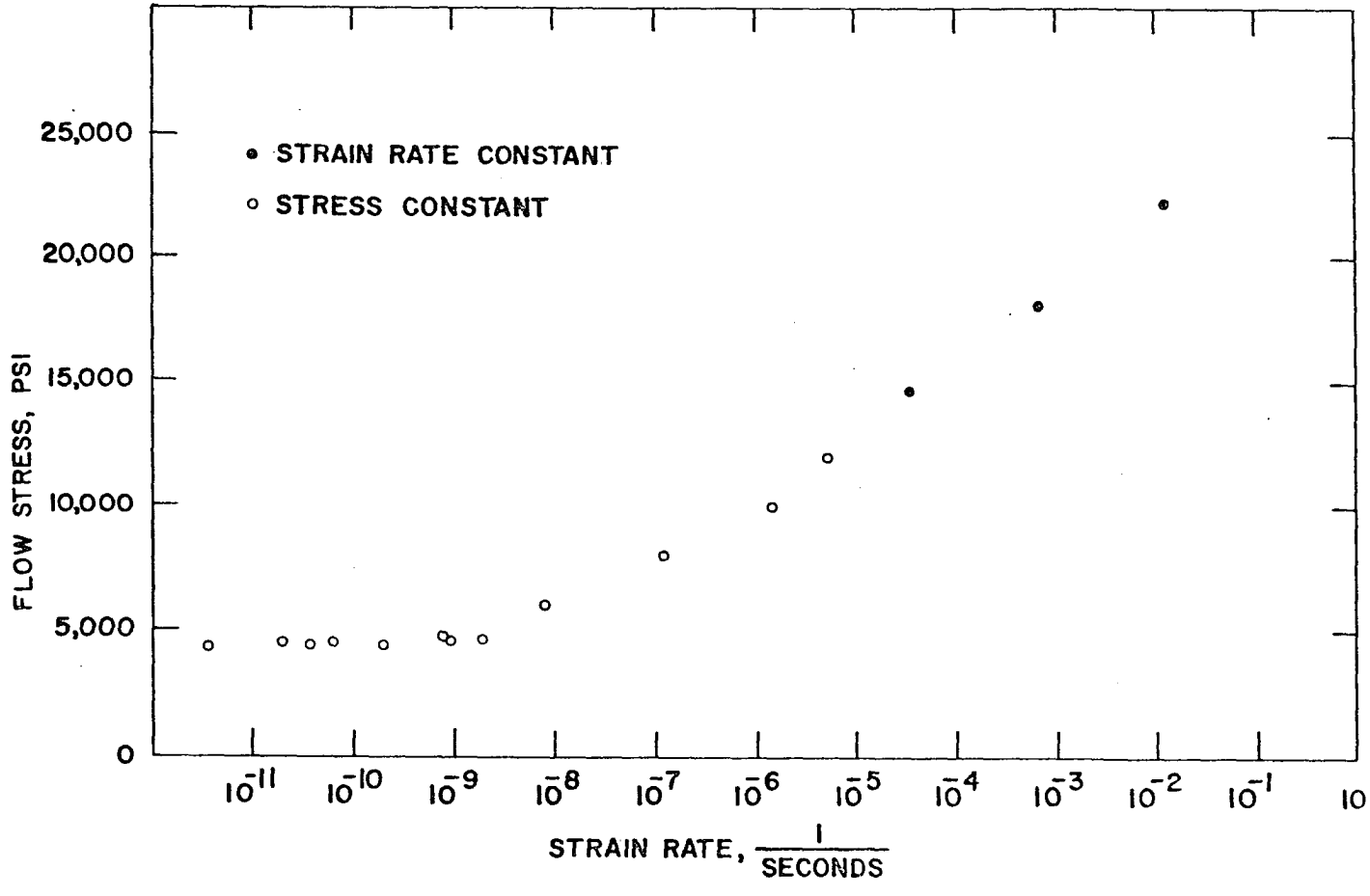

Figure 5. Variation of the flow stress of thorium-0.385 a/o carbon alloy with strain rate at zero strain and 273°K

carbon together with the 0.1 percent offset flow stress at 573°K. The values of the critical stress measured at 273°K and 300°K with 2% prestrain are shown in Table 4 for the same alloys together with the 2 percent offset flow stress measured at 433° and 573°K. It is evident that for a given carbon content and strain, there is some minimum stress required to produce plastic deformation. This minimum stress is independent of the method of measurement and is very nearly independent of temperature.

At stresses greater than the minimum, there exists a continuous functional relationship between flow stress and strain rate. This relationship may be determined by constant stress measurements or constant strain-rate measurements within the limits of the technique. Constant stress measurements over the range in strain rates from 10^{-12} to 10^{-6} per second are continuous with constant strain rate measurements over the range from 10^{-5} per second to 10^{-1} per second. A typical curve of the variation of flow stress with strain rate is given in Figure 5. Here is plotted flow stress versus strain rate for a thorium-0.385 a/o carbon alloy at zero strain and 273°K.

The thermally activated component at any temperature was

obtained by the expression,

$$\sigma^* = \sigma - \sigma_\mu . \tag{20}$$

Taylor (40) (Appendix 1) has shown that the effective shear stress in face centered polycrystals can be related to the tensile stress by the factor 3.1 as shown by

$$\tau^* = \frac{\sigma^*}{3.1} \tag{21}$$

where τ^* is the thermal component of effective shear stress. To avoid the effects of heavy work hardening, it was desired to evaluate τ^* at the lowest possible strain. Conversely, it was necessary to avoid the effects of the yield point phenomenon. In none of the alloys tested did the yield point persist to 2 per cent strain. Consequently, τ^* was evaluated at 2 percent strain. It was found that at every temperature τ^* increased linearly with carbon content but was not zero at zero carbon content, so that

$$\tau^* = K_1(C + 0.00285) \tag{22}$$

where C is the atom fraction carbon content, K_1 is a constant and -0.00285 is the intercept on the composition axis at which τ^* is zero. The effective carbon content, C_{eff}, then is given by

$$C_{eff} = C + 0.00285 . \tag{23}$$

The value 0.00285 is the carbon equivalent of all other

foreign atoms and defects in the thorium. The value obtained graphically is quite consistent with impurity content of the thorium used. This material contained enough oxygen to exceed the estimated 80 ppm solubility limit, approximately 30 ppm nitrogen, and about 100 ppm substitutional impurities. Since τ^* was directly proportional to the effective carbon content and τ^* varied linearly with temperature, it was possible to express τ^* with a function

$$\frac{\tau^*}{C_{eff}} = K_1\left(\frac{T_c - T}{T_c}\right) \qquad (24)$$

where K_1 is the value of the function at absolute zero and T_c is the temperature at which τ^* becomes zero. This function is plotted in Figure 6, as a function of temperature. The function deviates from linearity at about 300°K, and the extrapolated value of T_c was found to be 338°K. The value of K was found to be 12.8 Kg/mm^2 per atom percent carbon.

At temperatures approaching absolute zero there is little thermal activation and barriers to dislocation movement must be overcome by stress alone. The strength at 4.2°K is thus a measure of the stress required to surmount the barriers to dislocation motion. The 2 percent offset flow stress of thorium-carbon alloys at 4.2°K is shown as a function of carbon content in Figure 7. It is seen that

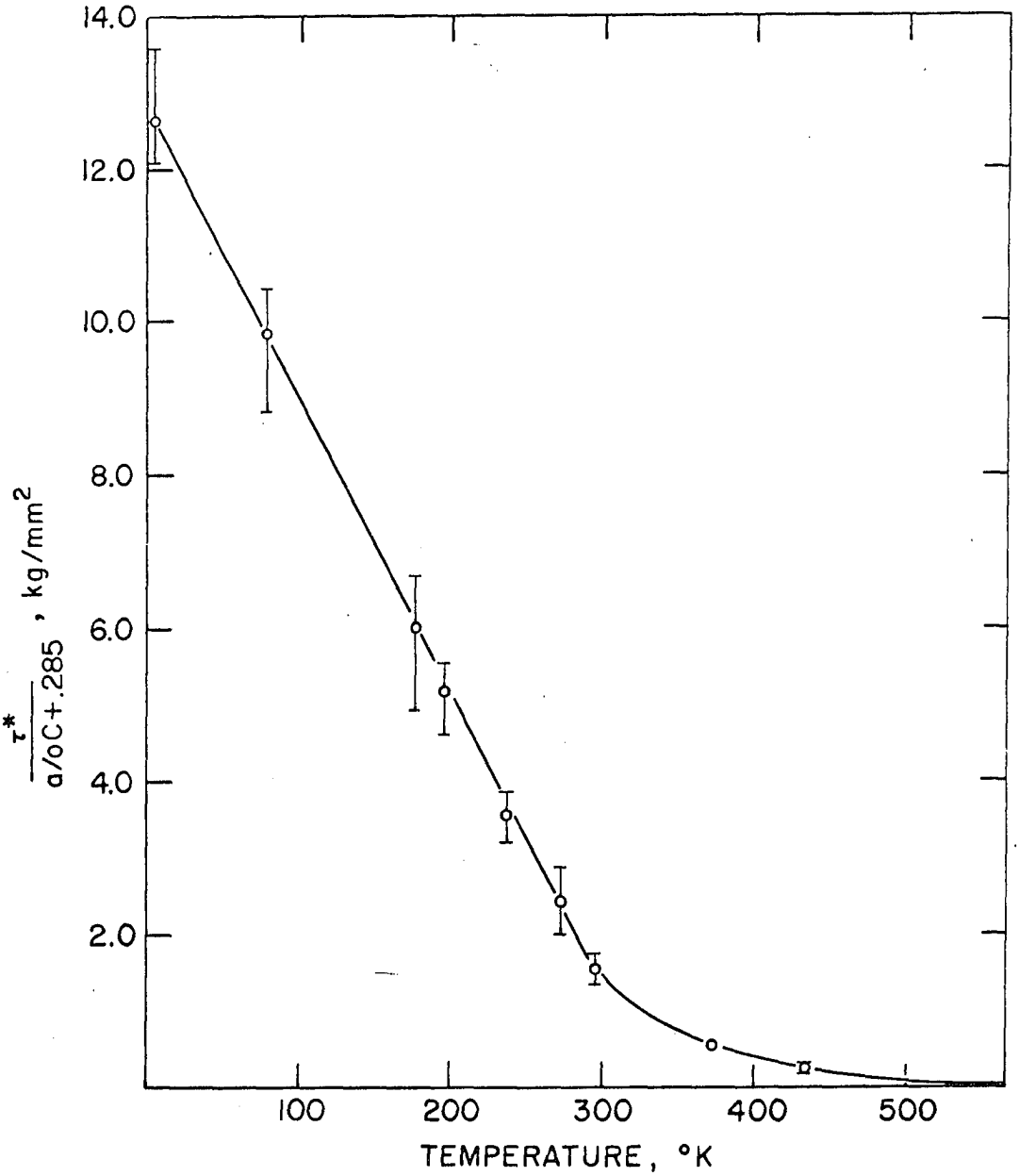

Figure 6. Variation with temperature of τ^*; normalized to unit effective carbon content

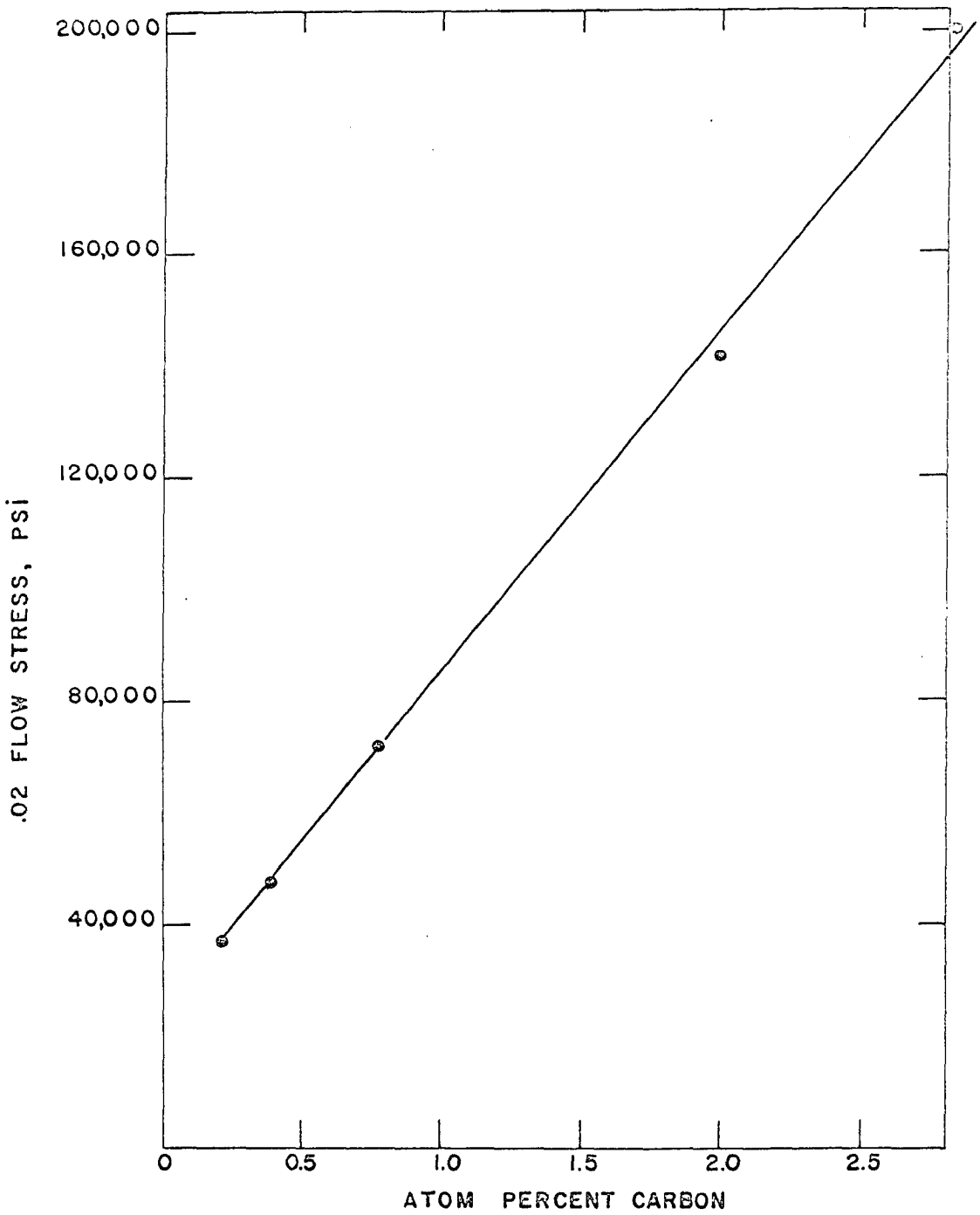

Figure 7. Variation of the 2 percent offset flow stress at 4.2°K with carbon content

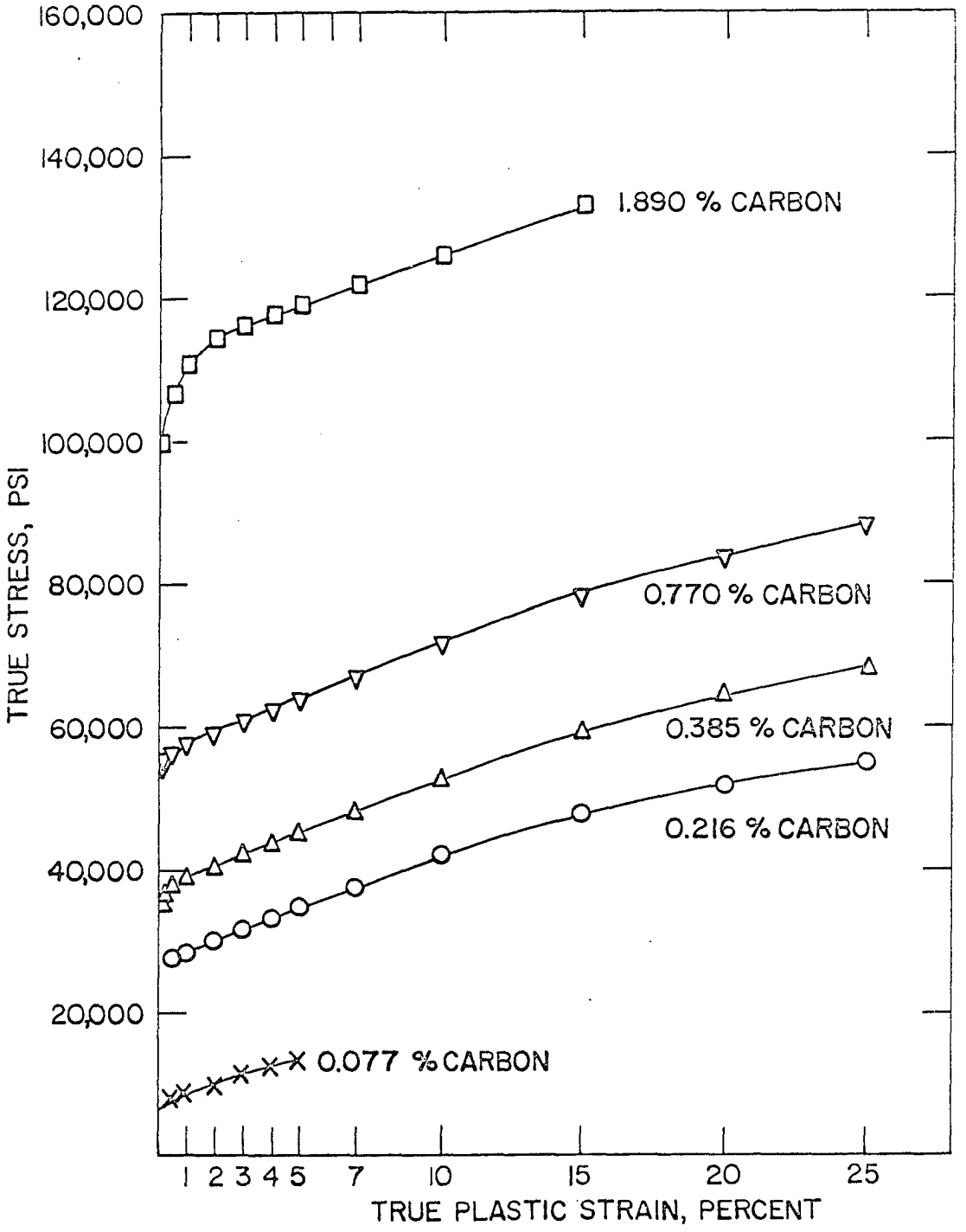

Figure 8. True stress-true strain curves for thorium-carbon alloys at 78°K

the strength of thorium increases rapidly and linearly with increased carbon content.

In order to determine the contribution of grain boundaries to the total strength, a series of extremely coarse grained thorium carbon alloys was tested. After heating at 1350°C for 45 hours, the 0.070" diameter specimens contained 1 to 3 grains per cross section. The 2 percent offset strength of the coarse grained material at 4.2°K was from 0 to 19 percent lower than that for the corresponding fine grained material. It was concluded that the contribution of the grain boundaries to the strength of thorium is small.

The increase in flow stress for a given strain at any temperature was, in general, the same for all carbon concentrations. The only exception to the above was observed in the low strain region at temperatures where the yield point was pronounced. The stress-strain curves for the series of thorium carbon alloys at 78°K is shown in Figure 8. Evidently, carbon does not significantly affect the work hardening of thorium metal.

The strain rate parameter, $\Delta\sigma/\Delta\ln\dot{\varepsilon}$, was evaluated at 2 percent strain as a function of temperature and carbon content. This parameter shows a maximum at approximately 250°K

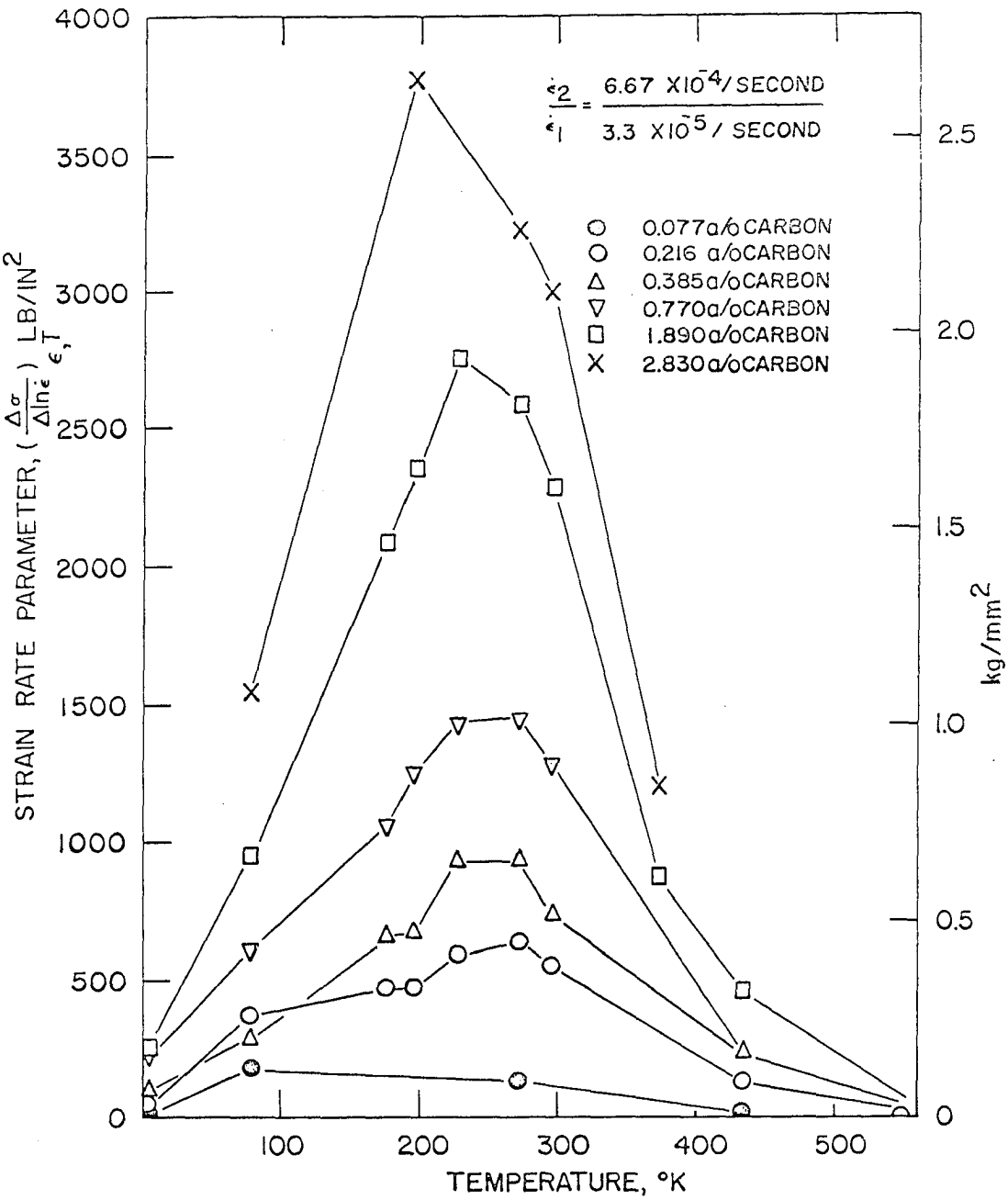

Figure 9. Variation of the strain rate parameter with temperature for thorium-carbon alloys

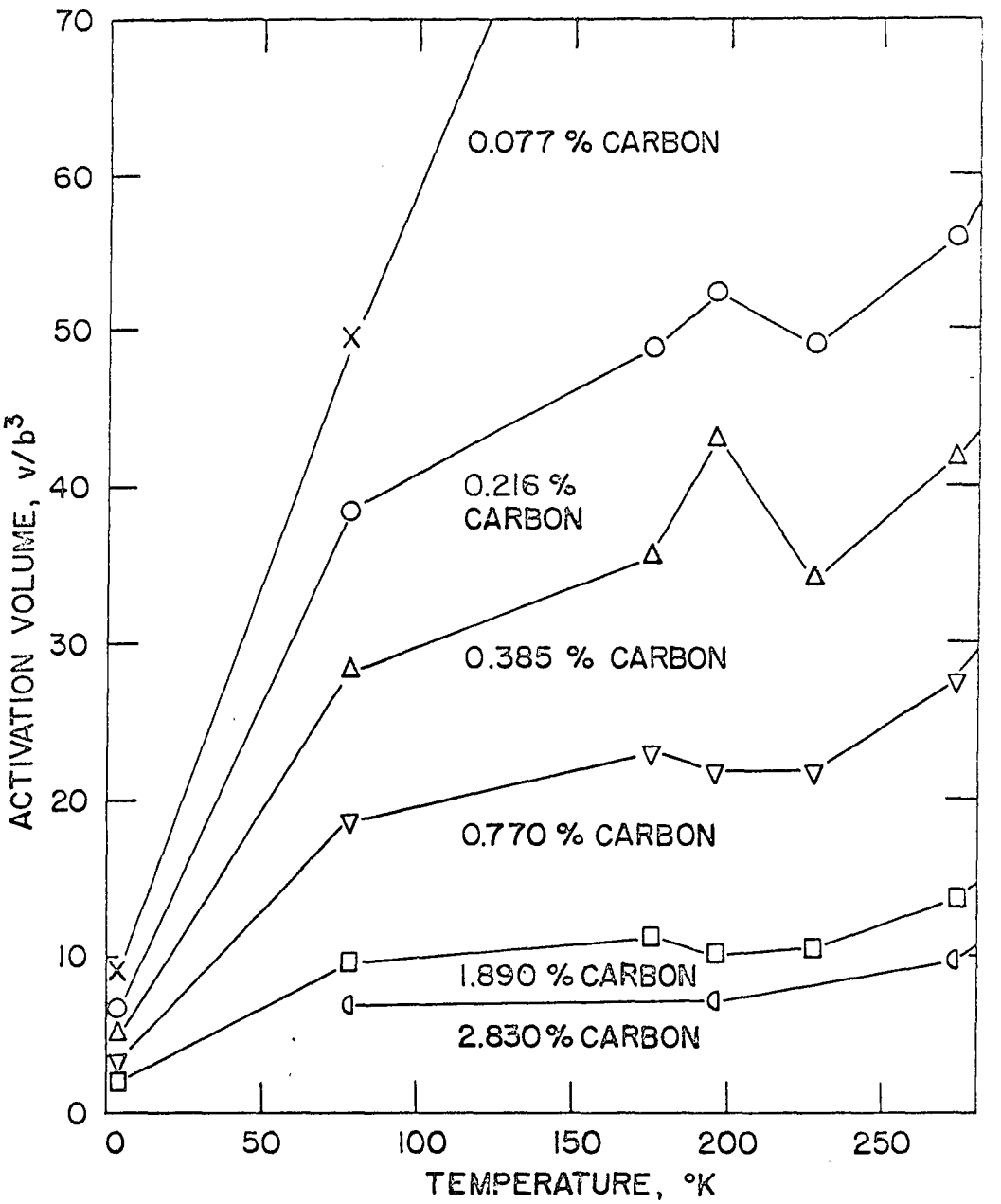

Figure 10. Variation of activation volume with temperature for thorium-carbon alloys

and increases linearly with increasing carbon content. The effect of temperature and carbon content on the strain rate parameter of thorium is shown in Figure 9.

The activation volume, v^*, as defined by the expression,

$$v^* = KT\left(\frac{\partial \ln \dot{\varepsilon}}{\partial \tau}\right)_{T,\varepsilon} \simeq KT\left(\frac{\Delta \ln \dot{\varepsilon}}{\Delta \tau}\right)_{T,\varepsilon}, \qquad (25)$$

was determined from the observed change in flow stress resulting from changes in strain rate. The values of activation volume measured in this work varied from approximately $2b^3$ to $60b^3$. These results are similar to the values reported for body centered cubic metals as summarized by Conrad (13). They are, however, quite low for a face centered cubic metal. The activation volume appears to be a function of carbon content. For the highest carbon content, the activation volume is nearly independent of temperature over the range from 78^oK to 273^oK, and increases rapidly above 273^oK. With decreasing carbon content, the temperature independent range becomes narrower and is finally lost. The variation of activation volume with temperature and carbon content is shown in Figure 10. Data from the nearly independent temperature range were used to obtain the relation between the activation volume and effective carbon content. A relation of the form

$$\frac{v^*}{b^3} = \frac{K_1}{C_{eff}} \tag{26}$$

was found, where v^* is the activation volume, b is the slip vector, C_{eff} is the effective atom fraction of carbon, and $K_1 = 1/4$. This function is plotted in Figure 11.

The expression (6) developed by Conrad and Wiedersich (11) was used to calculate the activation energy of deformation. The parameter $(\Delta\sigma/\Delta \ln \dot{\epsilon})_{T,\epsilon}$ was evaluated from strain rate change experiments while $(\Delta\sigma/\Delta T)_{\epsilon,\dot{\epsilon}}$ was obtained from the plot of flow stress as a function of temperature. Both of these parameters have been shown to increase linearly with carbon content. At each temperature these parameters were plotted as a function of effective atom percent carbon, giving relationships of the forms

$$(\Delta\sigma/\Delta \ln \dot{\epsilon})_{T,\epsilon} = K_1(\text{a/o } C_{eff}) \tag{27}$$

and

$$(\Delta\sigma/\Delta T)_{\dot{\epsilon},\epsilon} = K_2(\text{a/o } C_{eff}). \tag{28}$$

All of the experimental points were within five percent of the best straight lines. Since the activation energy is nearly proportional to the ratio of these two parameters, this showed that the activation energy for deformation was independent of composition. Values of the two parameters were taken from the best straight lines represented by

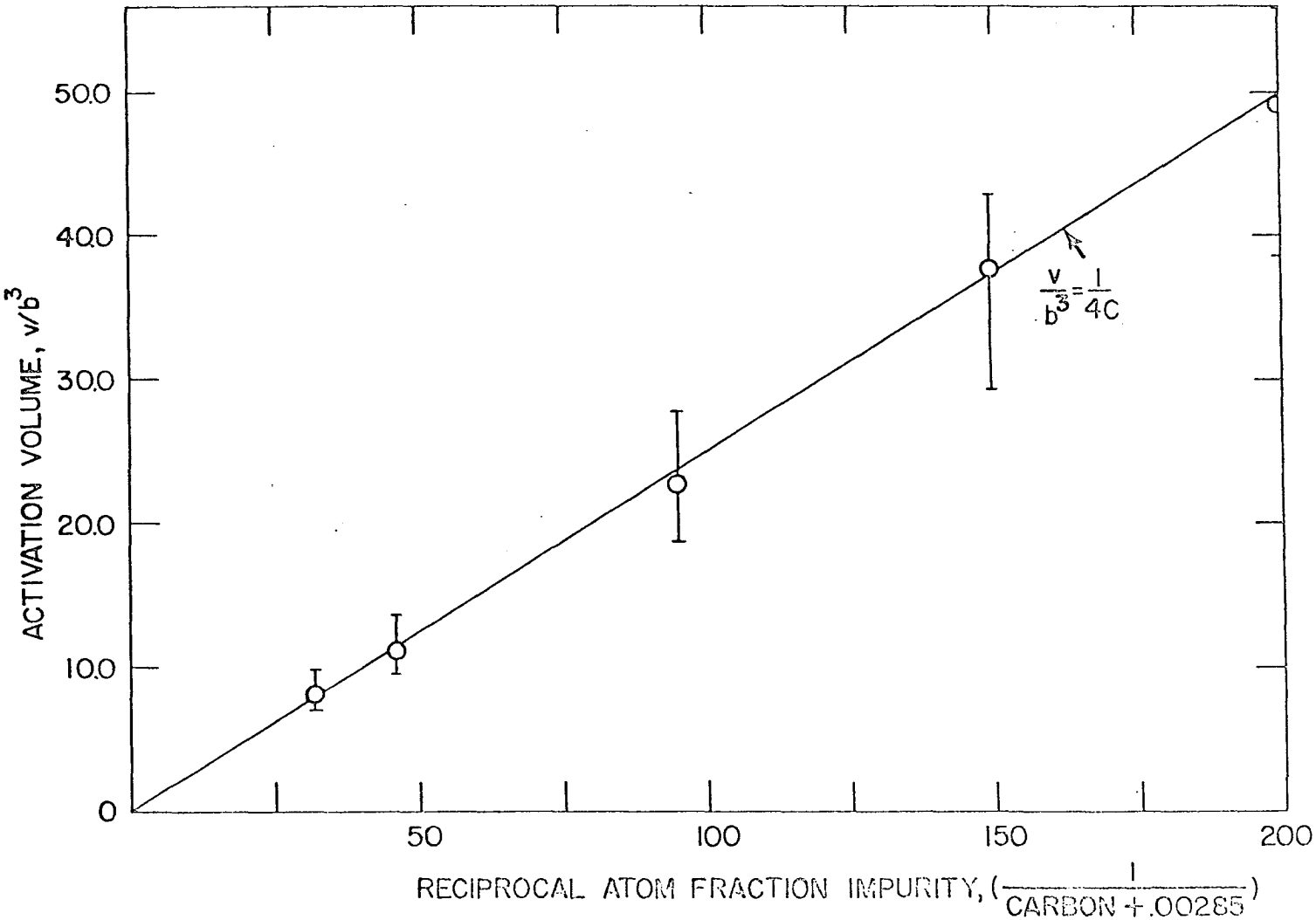

Figure 11. Dependence of the activation volume on the effective carbon content for thorium-carbon alloys

expressions (27) and (28) to calculate the activation energy.

The activation energy of deformation was found to increase linearly from nearly zero at 4.2°K to 0.55 electron volts at approximately 200°K. At temperatures above 200°K, the activation energy was found to be nearly constant. The variation of activation energy with temperature is shown in Figure 12.

A decrease in load on yielding, or yield point phenomenon, was observed between 78° to 430°K. The load-elongation curves for thorium containing 1.89 a/o carbon for the several temperatures covered by this investigation are shown in Figure 13. The yield point phenomenon was a maximum at approximately 250°K, and diminished with both increasing and decreasing temperature. The size of the yield point phenomenon was also observed to increase with increasing carbon content. Unlike the sharp yield point in iron, the upper yield point in thorium occurs only after appreciable, 0.001 to 0.005, plastic strain. In addition, the flow curve does not drop discontinuously to a lower yield point, but decreases smoothly to a minimum before it is increased by work hardening. Because of the smooth profile of the yield point in thorium, it is not adequately measured by the "drop in yield

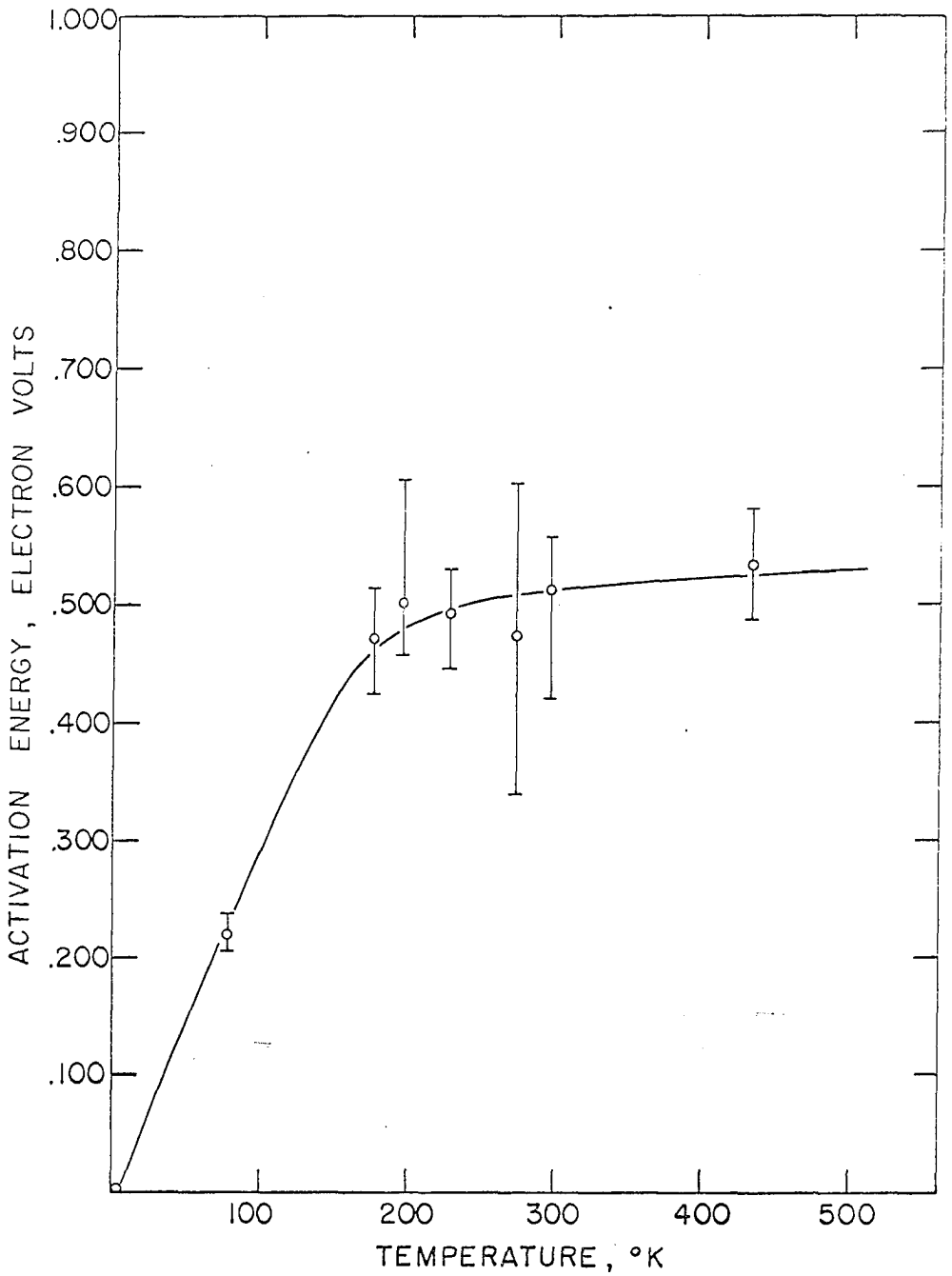

Figure 12. Variation with temperature of the activation energy for plastic deformation of thorium-carbon alloys

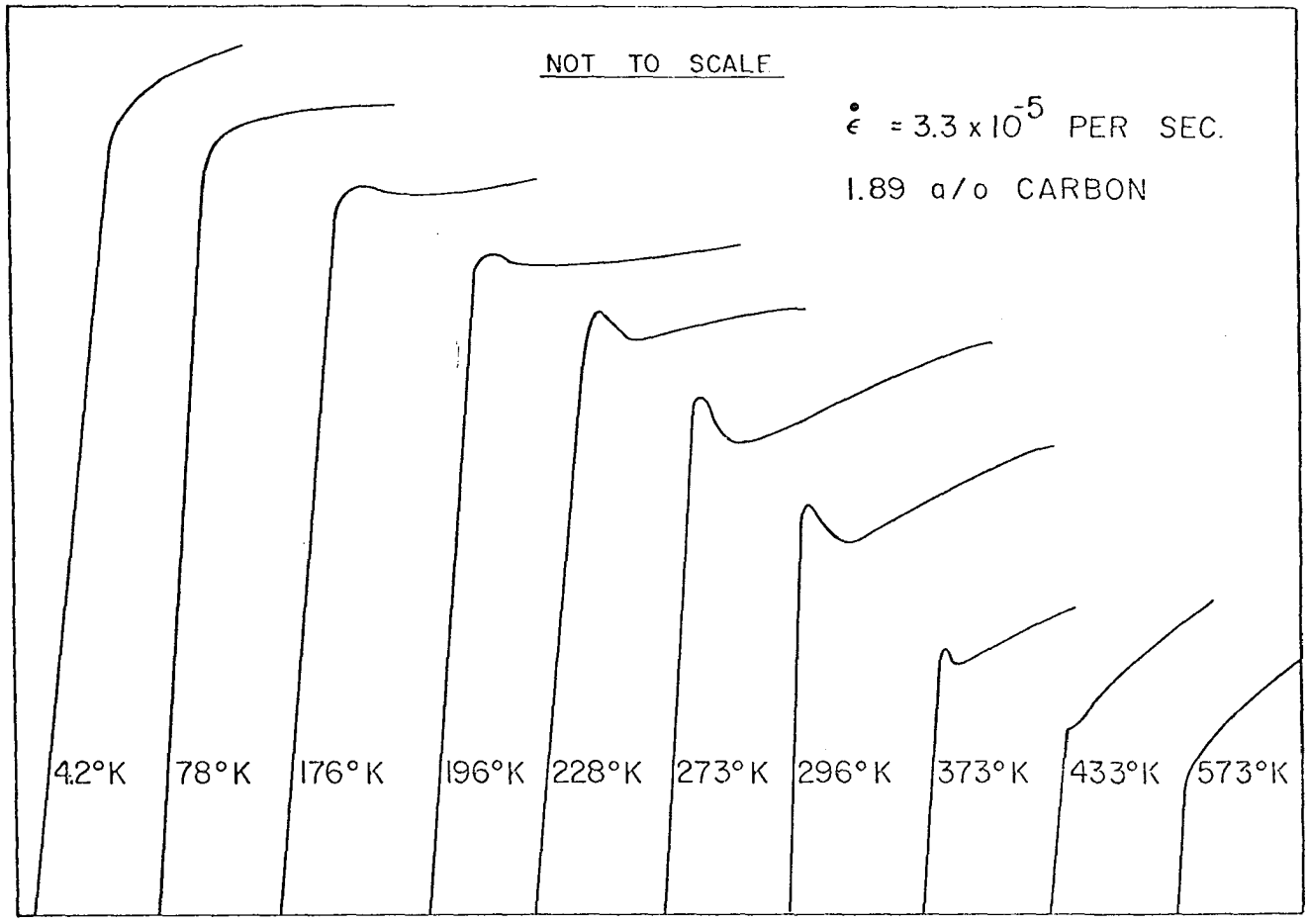

Figure 13. Load-elongation curves for thorium-1.89 a/o carbon alloy tested at several temperatures

point" parameter which has been used to characterize the yield point observed in iron. Accordingly, the yield point observed in this investigation was characterized by the extra energy required for deformation due to the occurrence of the yield point phenomenon. This yield point energy was evaluated by extrapolating the nearly linear portion of the flow curve back to the pre-yield elastic region and integrating graphically the area between the extrapolated curve and the observed flow curve. The yield point energy was found to be a maximum at approximately 250^{o}K and to decrease with higher and lower temperature. The yield point energy increased with increasing carbon content. Shown in Figure 14 is the variation of yield point energy with temperature and carbon content. Both the yield point energy and the strain rate parameter were observed to behave similarly with temperature and increase with carbon content. Consequently, a correlation between these two parameters was expected. The yield point energy increased logarithmically with increasing strain rate parameter as shown in Figure 15.

It was desired to observe the effect of variation in strain rate sensitivity upon the metallographically observable aspects of plastic deformation. Flat, electropolished

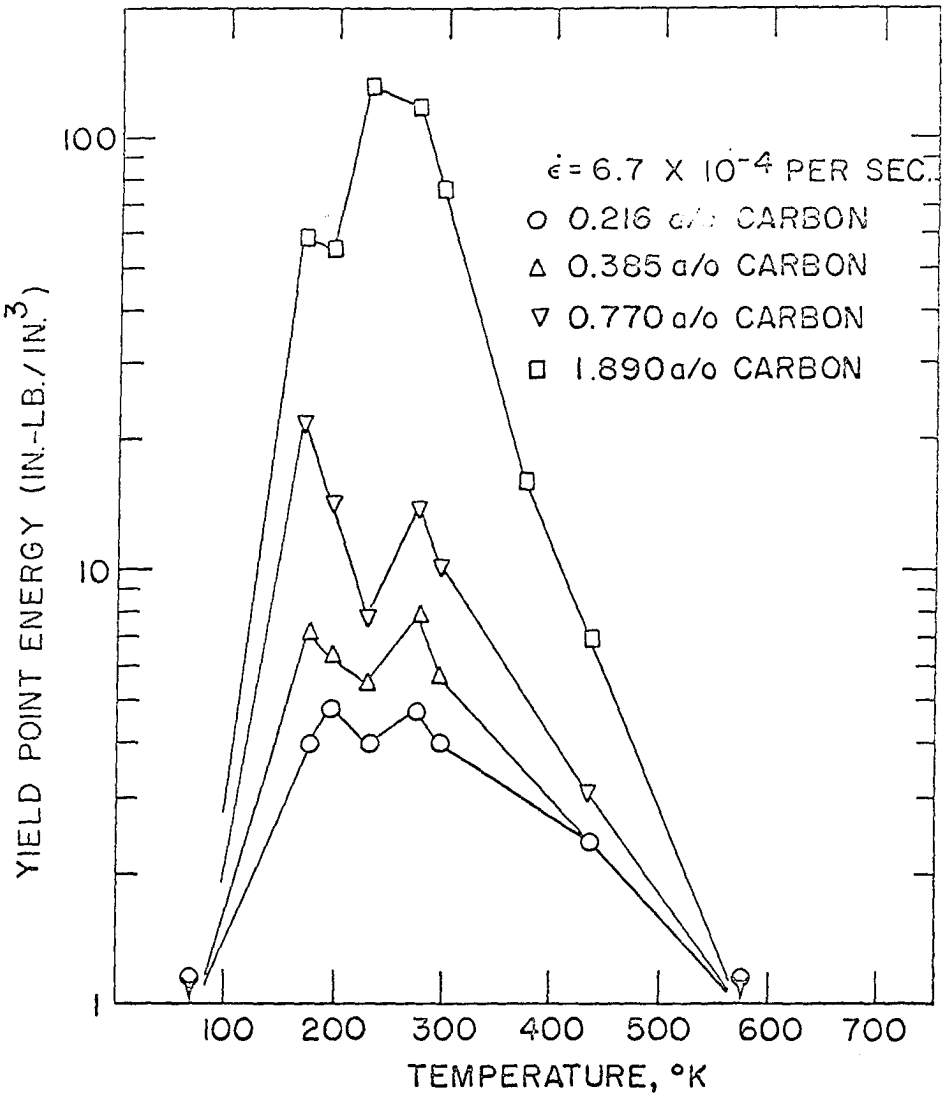

Figure 14. Variation of the yield point energy with temperature for thorium-carbon alloys

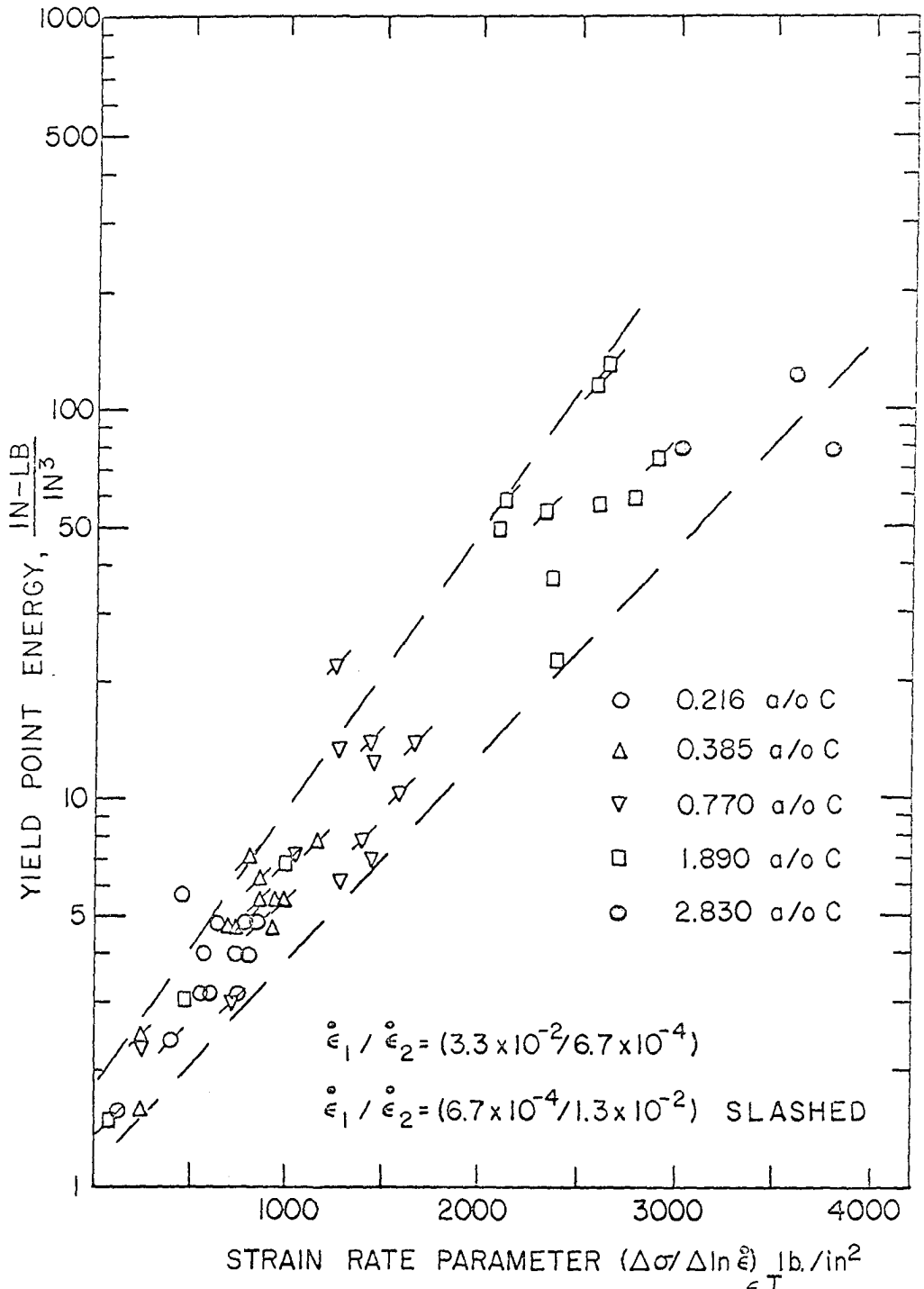

Figure 15. The relation between yield point energy and the strain rate sensitivity in thorium-carbon alloys

specimens containing 0.216, 0.770, and 1.89 a/o carbon were strained two percent at several temperatures and then examined metallographically. A definite relationship was observed between the character of the slip line traces and the strain rate sensitivity. Under conditions of high strain rate sensitivity, extremely fine slip was observed. Conversely, coarse slip was observed in specimens of low carbon content deformed at either high or low temperature. The distances between slip lines measured in specimens of several carbon contents deformed at a number of temperatures are shown in Table 5. This distance was plotted against the strain rate sensitivity parameter for the composition and temperature at which deformation occurred. The mean slip line spacing increased from approximately 1×10^{-5} inches at $\Delta\sigma/\Delta \ln \dot{\varepsilon} = 2600$ psi to 1×10^{-3} at $\Delta\sigma/\Delta \ln \dot{\varepsilon} = 100$ psi as shown in Figure 16.

The effect of grain size on the yield point behavior was studied by testing a series of 1.89 a/o carbon alloys which had been heated at elevated temperatures to produce large grain sizes. After coarsening, each sample was cooled to 730°C, the temperature at which the samples had originally been recrystallized, and held for one hour before furnace cooling to room temperature. In this way, differences

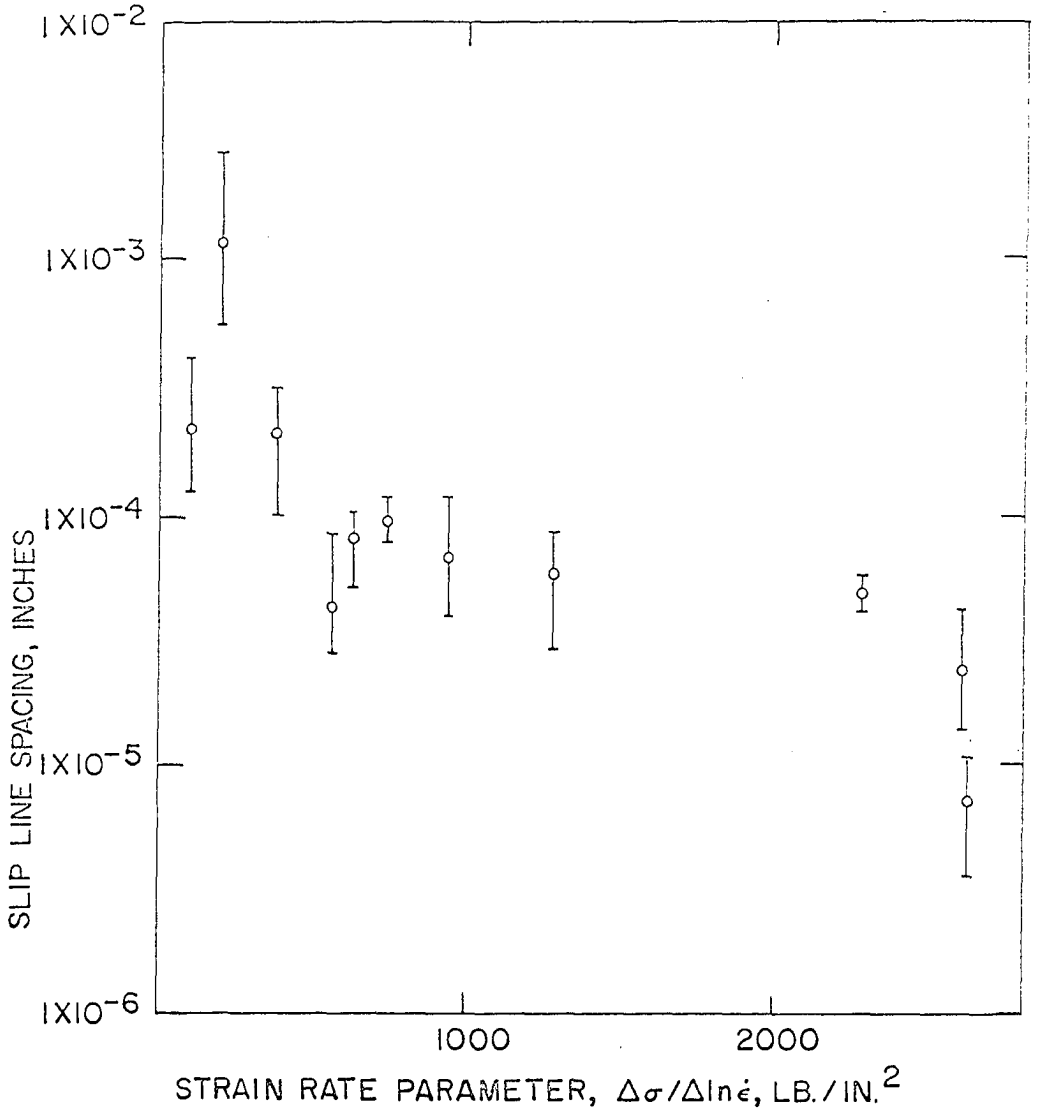

Figure 16. Variation of slip line spacing with strain rate sensitivity in thorium-carbon alloys

between the coarse grained and fine grained samples due to impurity distribution were minimized. A grain size determination was made on the unstrained portion of each specimen. The samples were then tested at 273°K and a strain rate of 3.3×10^{-5} per second. It was observed that the size of the yield point decreased from a value of 57.1 in-lb/in^3 for a grain size of 3200 grains per square mm to zero for a grain size of 500 grains per square mm. The annealing temperatures, grain sizes and resulting yield point energies are given in Table 6.

The effect of rapid cooling on the yield point was determined by the study of thorium-carbon alloys quenched from several temperatures. Specimens of the recrystallized thorium-carbon alloy containing 1.89 a/o carbon were subsequently reheated for one hour and quenched. The size of the yield point was studied as a function of the quenching temperature. It was found that reheating and quenching had no effect on the yield point until reheating temperatures above 575°C were used. The size of the yield point decreased rapidly with increasing reheat temperature and was zero for a specimen quenched from 765°C.

The recurrence of the yield point after straining at a

temperature of 273°K and subsequently heating was studied. Specimens containing 2.83 a/o carbon were strained 3 percent at 273°K, at a rate of 6.7×10^{-4} per second, held for one hour at a higher temperature, and then retested at 273°K. The yield point energy of the 2.83 a/o carbon alloy as recrystallized was measured at 273°K and found to be 124 in-lb/in^3. A small yield point was observed after heating. The yield point energy of 26 in-lb/in^3 was independent of reheating temperatures from 300°C up to 600°C, the highest reheat temperature used. Exploratory work had previously shown no yield point was observed in strained specimens reheated in the recrystallization range above 700°C. The load-elongation curve of thorium shows small "yield points" whenever the load is removed and reapplied or the strain rate is increased. Similarly, a "negative yield point" is observed when the strain rate is reduced. Orava *et al.* (27) observed similar yield points or transients in the load-elongation curve for titanium. The transient occurs with or without heating, and at 273°K, in the 2.83 a/o carbon alloy, was found to be approximately 16 in-lb/in^3. Thus, the return of yield point phenomenon, if it occurs at all in thorium, is small. It is also significant that

the size of the "yield point" was independent of the heating temperature. This is an indication that the yield point return is not diffusion related as is the case for iron. In this work the size of the transient was a maximum in the 228^{o}K to 273^{o}K range and decreased with higher and lower temperature. In the fine grained material, the energy of the transient was approximately 10-15 percent of the initial yield point energy. The effect appeared to be independent of strain except at the highest temperature. At 573^{o}K, the size of the transient was observed to increase with strain. For a given temperature and composition, transients resulting from strain rate changes in the high strain rate range were larger than those observed in the low range.

Table 3. Observed values of the athermal component of flow stress at zero strain

Carbon content (a/o)	Temperature 273°K	300°K	433°K	573°K
.216	3600 psi	3600 psi	4460 psi	4410 psi
.385	4300	4200	5100	5040
.770	5800	6000	7000	5740
1.890	12800	12600	11500	9990

Table 4. Observed values of the athermal component of flow stress at 2 percent strain

Carbon content (a/o)	Temperature 273°K	300°K	433°K	573°K
.216	9060 psi	8920 psi	8000 psi	8480 psi
.385	10100	9900	9000	9320
.770	11700	10950	11500	10840
1.890	16350	15500	16000	14140

Table 5. Summary of slipline observations on thorium carbon

Composition	Temperature	Average slip line spacing	$\Delta\sigma/\Delta\ln\dot{\varepsilon}$
1.890 a/o C	273°K	7.2×10^{-6} in	2600 lb/in^2
1.890	273	2.4×10^{-5}	2600
1.890	300	4.9×10^{-5}	2280
0.216	300	4.4×10^{-5}	561
0.770	300	5.9×10^{-5}	1280
0.216	300	6.0×10^{-5}	561
0.385	273	6.8×10^{-5}	938
0.770	273	8.2×10^{-5}	632
0.385	300	9.6×10^{-5}	744
0.216	78	2.2×10^{-4}	377
0.216	473	2.3×10^{-4}	250
0.0077	250	1.3×10^{-3}	200

Table 6. Effect of grain size on the yield point of Th-1.89 a/o C
Tested at a strain rate of 3.3×10^{-5} per second

Heat treatment	Grain size (grains/mm^2)	Yield point energy (in-lb/in^3)
As recrystallized	3200	57.1
840°C 1 hr. 730°C 1 hr. Fce. cool	2000	13.9
1000°C 1 hr. 730°C 1 hr. Fce. cool	1000	4.7
1180°C 1 hr. 730°C 1 hr. Fce. cool	500	0

DISCUSSION OF RESULTS

From the results of this work it is possible to draw conclusions about the manner in which dislocation movement in thorium containing carbon is impeded, i.e., the mechanism of strengthening. In order to simplify the problem, thermally activated processes which limit dislocation motion will be separated into two categories. The first category includes those processes which could occur in either a pure metal or an alloy. These are non-conservative motion of jogs, cross-slip of extended dislocations, the intersection of forest dislocations, and the overcoming of lattice friction. The observed properties of the electrotransport purified thorium place an extremely low upper limit upon the total contribution of all mechanisms not involving foreign atoms. Accordingly, no further consideration will be given the micro-processes of category one. The second category is restricted to those processes which require that foreign atoms be present. This group includes the overcoming of barriers caused by randomly dispersed substitutional or interstitial alloy atoms, regions of alloy segregation such as Gunier-Preston zones, Cottrell atmospheres, impurity stabilized stacking faults, and precipitates. It has been observed

that the flow stress, the strain rate dependence of flow stress, the temperature dependence of flow stress, and the activation volume are all strong functions of carbon content. Carbon atoms, then, in some form, impede the movement of dislocations. It is conceivable that the barrier could be any one or more of those listed in category two, and the problem is that of determining the manner of distribution of carbon in thorium. Elliot (8) has collected work on the thorium-carbon system. A continuous solid solution exists at high temperature between thorium metal and thorium monocarbide. In the range 1600°C to 1400°C a miscibility gap appears in which the equilibrium phases, down to room temperature, are the monocarbide and α thorium saturated in carbon. Below 700°C the mobility of carbon is extremely low. The diffusion coefficient at room temperature has been estimated from the measurements by Peterson (41) to be about 10^{-29} cm^2/second. Since, in this case, it is virtually impossible to achieve thermodynamic equilibrium at room temperature, the practical solubility limit of carbon in thorium is of interest. Mickelson and Peterson (7) report the solubility limit at room temperature to be 3500 ppm. This result was based on metallographic examination and precision lattice constant

measurements of thorium-carbon alloys cooled from 900° at a rate of about 7°C per hour. The lowest solubility limit in the literature is that of Smith and Honeycombe (42) who report a 2000 ppm limit at 350°C, from metallographic observations. These investigators plotted the amount of carbide observed as a function of carbon content. The extrapolation of this plot to zero carbide was taken as the solubility limit.

The work of Peterson et al. (43) provided information independent of arguments based on measurements of mechanical properties concerning the form of carbon in thorium. The residual resistivities of the thorium-carbon alloys used in this work were found to increase linearly with the carbon content to a concentration of at least 1000 ppm (1.89 a/o C). Mott and Jones (44) have discussed the effect of foreign atoms on the residual resistivity of metals. At low concentrations, the theoretical expression for the residual resistivity, ρ_o, is

$$\rho_o = \frac{m}{Ne^2} \frac{\nu x}{\Omega_o} A, \qquad (29)$$

where m is the electron mass, ν is the electron velocity, N is the effective number of electrons per unit volume, Ω_o is the specific volume of the solvent atom, x is the atom frac-

tion solute, and A is the effective scattering cross-section. Dilute solid solutions, in general, obey Equation 29 and a linear relation between the residual resistivity and the concentration is an indication that solute atoms act as randomly distributed electron scattering points.

Carbon segregation at extended dislocations would be expected to strongly influence the work hardening characteristics of thorium by making the cutting of forest dislocations more difficult. Indeed, it is difficult to imagine a process whereby the rate of work hardening is not influenced in some way by the presence of solute rich zones, or second phase particles. It has been observed that at 78°K, the flow stress versus strain curves of thorium carbon alloys from 0.0077 to 1.89 a/o carbon are parallel within the accuracy of the measurement. Thus, carbon does not affect the work hardening of thorium. This observation also suggests that segregation of carbon atoms does not occur.

It has been shown that the activation energy of deformation is independent of carbon content. The strain rate sensitivity parameter, $\Delta\sigma/\Delta\ln\dot{\epsilon}$, and the temperature dependence, $\Delta\sigma/\Delta T$, were observed to increase linearly with carbon and to extrapolate to zero at zero effective carbon content at all

temperatures. The rate of strengthening, $\Delta\sigma/\Delta c$, is also constant from 0.216 to 2.83 a/o carbon at all temperatures. Together, these four observations are convincing evidence that the mechanism by which carbon strengthens thorium does not change over the entire composition range from 0.216 a/o carbon to 2.83 a/o carbon. If the thorium-carbon solid solution deviated significantly from randomness, some nonlinearity would certainly be expected in going from a dilute solid solution to one approaching saturation.

All observed evidence leads to the conclusion that the strengthening of thorium is derived from an interaction between dislocations and randomly dispersed carbon atoms. It is instructive to compare the results obtained in this work with those predicted by Friedel (45) for random solid solutions. The model considers a dislocation moving under an applied stress through a field of randomly dispersed, stationary solute atoms. By an unspecified process the dislocation is pinned by solute atoms and moves by a succession of stress-assisted, thermally activated unpinning events. The variation of the elastic limit with temperature is predicted as a function of solute concentration and pinning energy. The model distinguishes between "dilute" and "not too dilute"

solutions, and each is considered separately. The dividing point between the two types is placed at 10^{-4} atom fraction solute. Friedel predicts that the elastic limit will vary with temperature according to the expression

$$\sigma = \sigma_i + (\sigma_c - \sigma_i)(1 - T/T_c)^n \qquad (30)$$

for $T \ll T_c$ where σ_i is the internal stress related to the athermal component, σ_μ, of this work, σ_c is the strength at absolute zero of temperature, T is the temperature, and T_c is the temperature intercept when the linear portion of the curve is extrapolated to $\sigma - \sigma_i = 0$. The values of n, σ_c and T_c vary with the concentration range. For the not too dilute case, n = 1, and a linear decrease in strength with increasing temperature is predicted until T approaches T_c. For compositions from 0.216 a/o C to 2.83 a/o C the thermally activated component of shear stress, τ^*, has been plotted as a single function of temperature

$$\frac{\tau^*}{(\text{a/o } C_{eff})} = 12.8\left(1 - \frac{T}{338}\right) \qquad (31)$$

as shown in Figure 6. Thus, the results of this work agree with the linear dependence of flow stress with temperature predicted by the Friedel model.

The flow stress of the electrotransport purified material appears to drop sharply in the temperature interval

between 4.2°K and 78°K, and then to decrease linearly with temperature. This behavior would appear to agree with the Friedel model for the dilute case where n - 3/2 in expression 30. Since the preparation of electro-transport purified material is a batch operation, it is entirely possible that the difference in strength observed between 4.2°K and 78°K could be due to small differences in residual impurities. For this reason no great significance is placed on the curvature of the flow stress-versus-temperature for the thorium .0077 a/o carbon alloy.

Friedel predicts that for the not too dilute case, the activation volume will be independent of stress and temperature and given by the expression

$$v^* \simeq \frac{\alpha b^3}{2c} \tag{32}$$

where b is the Burger's vector, c is the concentration of pinning solute, and α is a constant assumed to be from 1/3 to 1/2. For the very dilute case, the activation volume is a function of temperature according to the expression

$$v^* \simeq \frac{2b^3}{(1-T/T_c)^{\frac{1}{2}}} . \tag{33}$$

In Figure 10, it is seen that the activation volume becomes increasingly temperature dependent with decreasing carbon

content as predicted. Further, the plot of activation volume as a function of reciprocal effective carbon content in Figure 11 indicates that for $\alpha = \frac{1}{2}$, expression 32 is obeyed. The variation of the activation volume with temperature as the carbon concentration is increased was particularly interesting. The most dilute alloy showed a strongly temperature dependent activation volume and the most concentrated alloy an activation volume that was independent of temperature. Between the extremes are seen a series of four inflected curves which represent a transition from one limiting case to the other.

The model also predicts that, for the not too dilute concentrations, the activation energy will be independent of concentration and linear in temperature up to nearly T_c. A linear dependence of activation energy with temperature was observed as predicted. The activation energy, however, increases linearly with temperature only to about 200°K and then remains nearly constant. The value of T_c as determined by the extrapolation of the shear stress temperature curve in Figure 6 is 338°K. The measurement of stress is direct, and conversely, the activation energy is a derived quantity. Accordingly, greater reliance must be placed on the value of

T_c = 338°K, which was obtained from the variation of flow stress with temperature. The results, then, do not agree with the model in that the linear dependence of strength with temperature persists to higher temperature than does the linearity of activation energy. This discrepancy is not believed to be critical in view of the fact that rather large errors are involved in the measurement of the activation energy. In addition, a number of "order of magnitude" estimates were involved in the development of the model.

The mechanism by which carbon atoms impede dislocations will now be considered. Fleischer (20) has reviewed the subject of solid solution hardening and has summarized some of the theories dealing with interactions between dislocations and solute atoms. One possible interaction is a relaxation between the dislocation stress field and the elastic distortion caused by the solute atom. The model of Cottrell (46), modified by Bilby (47), Nabarro (48), and Eshelby (49) allows the calculation of elastic interaction energy ΔE between an edge dislocation and a solute atom by the expression

$$\Delta E = \frac{4(1+\nu)\mu b r_o^3 \sin\theta}{3(1-\nu)L} \frac{1}{a_o} \frac{da_o}{dc} \qquad (34)$$

where μ is the shear modulus, ν is Poisson's ratio, b is the slip vector, r_o is the radius of the empty hole, a_o is the lattice parameter, c is the concentration of solute, L is the distance from the solute atom and the edge dislocation, and θ is the angle between the slip plane and the plane through the dislocation and solute atom. Values for the shear modulus and Poisson's ratio were estimated to be 2.5×10^{11} dynes per square centimeter and 0.27 respectively from the work of Armstrong et al. (39). The radius of the empty octahedral hole was calculated from the hard sphere approximation to be 0.414 times the radius of the thorium atom. The specific increase in lattice parameter with carbon content, $1/a_o \cdot da_o/dc$, was calculated from the work of Mikelson and Peterson (7) to be 0.111 where the carbon concentration is in atom fraction. The interaction energy between an edge dislocation and a carbon atom in an octahedral hole one atomic plane directly below the dislocation was calculated. On the basis of this expression the interaction energy was 0.016 electron volts. This result is, of course, negligible compared to the observed activation energy of 0.55 electron volts.

The method of Cochardt et al. (19) has been used by Fleischer (50) to calculate the elastic interaction between a screw

dislocation and a defect. The resulting interaction energy is, in general, zero, when the defect produces a spherical distortion such that $\varepsilon_1 = \varepsilon_2 = \varepsilon_3$. To the first approximation, spherical distortion must occur if the solvent atoms are placed symmetrically around the solute atom. In the face centered cubic lattice, the above condition is met for both the tetragonal holes and for the octahedral holes. The elastic interaction model predicts that a solute atom producing a spherical distortion in the lattice will, in general, be less effective as a strengthener than one producing a tetragonal distortion. The strengthening at absolute zero per unit alloy addition, $d\tau/dc$, expressed in terms of the shear modulus, μ, is used to distinguish between "rapid" and "gradual" hardeners. According to the Fleischer model "rapid" hardeners produce large tetragonal lattice strains and $d\tau/dc > 2\mu$. On the other hand, "gradual" hardeners produce spherical strains and $d\tau/dc < 1/10\ \mu$ in metals. In Figure 7 is shown the variation of 2 percent offset flow stress of thorium at 4.2°K as a function of carbon content. If it is assumed that

$$\tau = \sigma/2 \tag{35}$$

and

$$\mu = \frac{E}{2(1+\nu)} \tag{36}$$

where τ is the shear stress, σ is the tensile stress, μ is the shear modulus, E is Young's modulus for thorium and is equal to 10.0×10^6 psi, and ν is Poisson's ratio and is equal to 0.27, then

$$\frac{d\tau}{dc} = 0.97\mu \quad . \tag{37}$$

If it is assumed that $\tau = \sigma/3.1$ and

$$\mu = 1/3(C_{11}+C_{12}-C_{44}) \tag{38}$$

where μ is the shear modulus for the $\{111\}\langle 110\rangle$ system, and C_{ik} are the elastic constants for thorium determined by Armstrong et al. (39), then,

$$\frac{d\tau}{dc} = 0.50\mu. \tag{39}$$

The rate of strengthening, then, approaches that of the "rapid" hardeners, and it can be surmised that the interaction between carbon atoms and dislocations is strong. This is borne out by the magnitude of the observed activation energy. The interaction energy is at least as large as the measured activation energy, 0.55 electron volts, and probably lies closer to one electron volt. An interaction of this magnitude can not be easily explained by an elastic interaction argument.

Fleischer (51) has proposed that solute atoms might act

as "hard" or "soft" spots in the lattice which interact elastically with the stress field of the dislocation. This approach is attractive because it avoids the zero interaction energy which results when the elastic interaction is calculated between an interstitial atom and a screw dislocation in a face centered cubic metal. There is, however, no realistic way in which to evaluate this modulus effect. Macroscopic measurements could not be expected to describe localized changes in modulus.

Since at this point it is not possible to explain the size of the carbon-dislocation interaction in terms of current theories, the carbon-thorium interaction will be considered. The monocarbide of thorium has a sodium chloride type structure with carbon atoms in octahedral holes and surrounded by six thorium nearest neighbors. Thorium and thorium monocarbide form a continuous series of solid solutions and thus it is most likely that the carbon in solid solution in thorium will be in an octahedral hole.

It is possible to show by a simple thermodynamic argument that the interaction of carbon with the nearest neighbor thorium atoms is strong. An energy can be calculated for each thorium-carbon interaction by considering the energy to

break carbon-carbon bonds in graphite and subsequently form thorium-carbon bonds in thorium monocarbide. The enthalpy of sublimation of graphite at 25°C is given by Kubaschewski and Evans (52) to be 170.0 kilocalories per mole. The enthalpy of formation of thorium monocarbide at 25°C is, according to Aronson (53) -29 kilocalories per mole. The energy to form six thorium-carbon bonds is 199 kilocalories per mole, 33.2 kilocalories per bond, or 1.44 electron volts per bond. The activation energy for the diffusion of carbon in thorium is also a measure of the energy required to move a carbon atom through an energy saddle point to an adjacent octahedral hole. Peterson (41) reports this value to be 38 kilocalories. This figure is high for the diffusion of an interstitial in a face centered cubic metal particularly when the large atomic diameter and low elastic constants of thorium are taken into account. For example, Jost (54) gives the activation energy for the diffusion of carbon in γ iron to be 32-36 kilocalories. This is another indication of strong bonding between carbon and thorium.

Rundle (55) has discussed the interstitial phases MX, where M is an A subgroup metal in the III, IV, V, and VI groups of the periodic table, and X is carbon, nitrogen, or

oxygen. He notes that these phases in general form sodium chloride structures regardless of the metal structure or atom size. He further points out that although the metal-metal distances are greater in the MX phase than in the pure metal, the interstitial compound phase is always harder and has a higher melting point. In order to explain these observations, Rundle proposed a covalent bonding mechanism whereby the interstitial atom could form resonating bonds with the six nearest metal neighbors. Covalent bonds are selective in their number, length, and direction. These characteristics are reflected in the structure and properties of thorium monocarbide. The formation of covalent thorium-carbon bonds in solid solution could well explain the dramatic strengthening of thorium by carbon. The stress field of an edge or screw dislocation moving near a carbon atom covalently bonded to six nearest thorium neighbors must change the length, direction, and number of the directed bonds. Such a process could require energy of the order of an electron volt.

The athermal component of the flow stress also increases with increasing carbon content. The observed dependence of the athermal component was of the form

$$\sigma_\mu = K_1 = K_2(C_{eff})^n \qquad (40)$$

where K_1 is a function of strain, K_2 is equal to approximately 5000 psi/a/oC_{eff}, and n is equal to or slightly less than 1. Friedel predicted that the solute atoms at some distance from the slip plane would give rise to an athermal resistance to dislocation motion. The predicted expression for the athermal component in the not too dilute case is

$$\sigma_\mu \simeq \frac{2U_m}{b^3} C^{4/3}. \qquad (41)$$

Where U_m is the maximum binding energy. If the maximum binding energy is taken to be 1 electron volt, then the predicted athermal component is of the same order of magnitude as that observed. The Friedel expression for the athermal component predicts a slightly stronger dependence on solute concentration than was observed. There are, however, other factors contributing to the athermal component which are not taken into account by the Friedel model. A few of these factors are grain size, the presence of oxide precipitates, and dislocation density.

The observed dependence of the athermal component upon solute concentration also agrees qualitatively with the findings of Wynnblatt and Dorn (56) on iron-2% manganese alloys. They report that, although the thermally activated component was independent of purity, the athermal component

increased sharply with total carbon plus nitrogen content. It would appear that the addition of solute atoms to a metal always makes some contribution to the athermal component of strength. As shown by this work and the work of Wynnblatt and Dorn (56), the thermally activated component may or may not be affected.

The yield point behavior observed in thorium is similar, at least in some respects, to that of other metals which display yield point phenomena. The magnitude of the yield point was much larger in the fine-grained than in coarser-grained specimens and disappeared when there were less than 50 grains along a diameter of the tensile specimen.

The effect of grain size upon the yield point observed in this work agrees qualitatively with the findings of Christ et al. (57) on zone refined iron. They report that the upper yield point was observed only when the number of grains through the minimum dimension of the specimen was from 12 to 16. A number of other investigators are cited who report the loss of the upper yield point when the average grain diameter reached some critical fraction of the minimum specimen dimension.

The decrease in magnitude of the yield point due to

quenching is also evidently general. Adair et al. (58) studied the yield behavior of vacuum melted iron containing 150 ppm total interstitials and with a grain size of about 0.026 mm in diameter. Samples were recrystallized at 700°C, either furnace cooled or quenched, and subsequently tensile tested. The furnace cooled specimens yielded sharply when tested at 242°K while the quenched specimens yielded smoothly, showing only an inflection rather than a drop in the load elongation plot. The authors concluded that the presence of impurities at the grain boundaries strongly locked dislocation sources and that strong locking results in large, sharp yield point.

The dependence of yield point behavior on grain size and on grain boundary segregation has also been noted in hexagonal closest packed metals. Weinstein (28) reports that abrupt yielding in zirconium containing about 150 ppm interstitial impurities was favored by slow cooling after recrystallization and by small grain size. Attempts to restore the yield point by heating strained speciment in the temperature range from 200°C to 300°C were unsuccessful. Weinstein (28) concluded that the yield point behavior of zirconium agreed with the dynamic model of yielding proposed by Hahn (59).

Although the smooth yielding observed in thorium differs from the abrupt yielding generally reported for body centered cubic metals, it is not unique. Van Torne and Thomas (60) show load elongation plots for niobium which are smoothly rounded at the upper yield point and decrease gradually to a minimum. The authors term this behavior "semi-discontinuous" yielding. It is, in the immediate vicinity of the yield point, almost identical to that observed in thorium carbon alloys. The correlation between yield point size and strain rate sensitivity observed in this work is evidently general. Hahn (59) has collected the results of several investigators to show that prominent yield points occur when the strain rate sensitivity is large. Evidently the only aspect of the yield point in thorium that is unique is the observed relation between the yield point energy and the slip line spacing. The ratio of yield point energy to the corresponding slip line spacing estimated from Figure 16 was found to be nearly constant and equal to approximately 8.0×10^{-4} in-lb/in^2. For the largest yield points, the value of the ratio nearly doubled. Since the measurements of the smallest slip line spacings were made at the limit of resolution, there is reason to believe that the actual slip line spacings were smaller

than those reported. Hence, the relation may hold true for even the largest yield points.

In the results of this investigation can be found evidence to support both the dynamic model of Hahn (59) and the static model due to Petch (61). The relation between the strain rate parameter and the size of the yield point is in agreement with the Hahn (59) model. Further, the correlation between the size of the initial yield point and that of the transient is evidence of some dynamic contribution to the yield point. Other observations argue that the upper yield point is associated with the propagation of slip across grain boundaries as proposed by Petch (61). Those factors which would appear to increase the stress required to propagate slip from grain to grain contribute to the size of the yield point. These factors are small grain size, segregation at the grain boundaries, and fine slip.

CONCLUSIONS

At temperatures below 550°K, the flow stress of thorium-carbon alloys can be resolved into a thermally activated component and an athermal component. The thermally activated component increases linearly with increasing carbon content. The thermally activated flow stress also increases with decreasing temperature and at 4.2°K is much larger than the athermal component. This thermally activated component leads to a strain rate variation of the flow stress. The strain rate sensitivity shows a maximum at approximately 250°K and increases linearly with carbon content. Carbon strengthens thorium primarily through an interaction of dislocations with random solute carbon atoms. The strength of this interaction appears to be about one electron volt.

The athermal component was observed to be nearly temperature independent over the temperature range from 273°K to 573°K. It was found to increase with carbon content and with strain. The increase of flow stress with strain is independent of carbon content.

The yield point phenomenon in thorium increases with increasing carbon content and is observed in the same temperature range as the largest strain rate sensitivity. The

yield point is much larger in fine-grained than in coarse-grained specimens and disappears in very coarse-grained or in quenched specimens.

BIBLIOGRAPHY

1. Smith, J. F. Physical constants, crystal structure, and thermodynamic properties. In Wilhelm, H. A., ed. The metal thorium. pp. 133-147. Cleveland, Ohio, American Society for Metals. 1958.

2. Milko, J. A., Adams, R. E., and Harms, W. O. Mechanical properties of thorium and high thorium alloys. In Wilhelm, H. A., ed. The metal thorium. pp. 186-216. Cleveland, Ohio, American Society for Metals. 1958.

3. Klieveneit, Harold. Plastic properties of thorium. Unpublished M.S. thesis. Ames, Iowa, Library, Iowa State University of Science and Technology. 1960.

4. Schwope, A. D., Muehlenkamp, G. T., and Marsh, L. L. Mechanical and metallurgical properties of thorium. United States Atomic Energy Commission Report BMI-784 [Battelle Memorial Inst., Columbus, Ohio]. 1952.

5. Young, J. D. The creep of thorium near room temperature. Unpublished M.S. thesis. Ames, Iowa, Library, Iowa State University of Science and Technology. 1964.

6. Milko, J. A. Impact behavior of thorium. United States Atomic Energy Commission Report ORNL-2122 [Oak Ridge National Lab., Tenn.]. 1956.

7. Mickelson, R. and Peterson, D. Solubility of carbon in thorium. American Society for Metals Transactions 50: 340-347. 1958.

8. Elliot, R. P. Constitution of binary alloys. First supplement. New York, N.Y., McGraw-Hill Book Company. 1965.

9. Cottrell, A. H. Dislocations and plastic flow in crystals. 1st ed. London, England, Oxford University Press. 1953.

10. Conrad, H. Thermally activated deformation of metals. Journal of Metals 16: 582-588. 1964.

11. Conrad, H. and Wiedersich, H. Activation energy for deformation of metals at low temperatures. Acta Metallurgica 8: 128-130. 1960.

12. Schoeck, G. The activation energy of dislocation movement. Physica Status Solidi 8: 499-507. 1965.

13. Conrad, H. Yielding and flow of the B.C.C. metals at low temperatures. In National Physical Laboratory Symposium No. 15: 476-512. London, England, Her Majesty's Stationery Office. 1963.

14. Gregory, D. P. Temperature variation of flow stress in body centered cubic metals. Acta Metallurgica 11: 455-461. 1963.

15. Mordike, Barry L. and Haasen, Peter. The influence of temperature and strain rate on the flow stress of α iron single crystals. Philosophical Magazine 7: 459-474. 1962.

16. Basinski, Z. S. Thermally activated glide in face centered cubic metals and its application to the theory of strain hardening. Philosophical Magazine 4: 393-431. 1959.

17. Wessel, E. T. Some exploratory observations of the tensile properties of metals at very low temperatures. American Society for Metals Transactions 49: 149-169. 1957.

18. Fleischer, Robert L. Solution hardening by tetragonal distortions: application to irradiation hardening in F.C.C. crystals. Acta Metallurgica 10: 835-824. 1962.

19. Cochardt, A. W., Schoeck, G., and Wiedersich, H. Interaction between dislocations and interstitial atoms in body centered cubic metals. Acta Metallurgica 3: 533-537. 1955.

20. Fleischer, R. L. Solid solution hardening. In Peckner, D., ed. The strengthening of metals. pp. 93-140. New York, N.Y., Reinhold Publishing Corporation. 1964.

21. Williamson, G. K. and Smallman, R. E. X-ray evidence for the interstitial position of carbon in α iron. Acta Crystallographica 6: 361-362. 1953.

22. Bechtold, H. Tensile properties of annealed tantalum at low temperatures. Acta Metallurgica 3: 249-254. 1955.

23. Seeger, A., Schiller, P, and Krönmüler, H. Observations of interstitial atoms in FCC metals. Philosophical Magazine 5: 853-857. 1960.

24. Van Bueren, H. G. Imperfections in crystals. 2nd ed. Amsterdam, The Netherlands, North-Holland Publishing Company. 1961.

25. Geil, Glenn W. and Carwile, Nesbit L. Tensile properties of copper, nickel, and some copper nickel alloys at low temperature. National Bureau of Standards Circular 520: 67-95. 1955.

26. Seeger, A. The mechanism of glide and work hardening in face centered cubic and hexagonal close-packed metals. In Fisher, J. C., Johnston, W. G., Thompson, R., and Vreeland, T., Jr., eds. Dislocations and mechanical properties of crystals. pp. 243-329. New York, N.Y., John Wiley and Sons. 1957.

27. Orava, R. N., Stone, G., and Conrad, H. The effects of temperature and strain rate on the yield and flow stresses of α-titanium. American Society for Metals Transactions 59: 171-184. 1966.

28. Weinstein, D. Yield point occurrence in polycrystalline alpha zirconium. Electrochemical Technology 4: 307-312. 1966.

29. Flinn, P. A. Solid solution hardening. In Hardwood, J., ed. Strengthening mechanisms in solids. pp. 17-50. Cleveland, Ohio, American Society for Metals. 1962.

30. Sonon, D. E. and Smith, G. V. The effect of interstitial impurities, grain size, and temperature on the plastic flow of type 330 stainless steel. American Society for Metals Transactions 58: 353-359. 1965.

31. Boniszewski, T. and Smith, G. C. The influence of hydrogen on the plastic deformation, ductility, and fracture of nickel in tension. Acta Metallurgica 11: 165-178. 1963.

32. Peterson, D. T., Krugg, W. E., and Schmidt, F. A. The preparation of high purity thorium by the magnesium reduction of thorium tetrachloride. Journal of the Less Common Metals 7: 288-295. 1964.

33. Peterson, D. T., Schmidt, F. A., and Verhoeven, J. D. Electrotransport of carbon, nitrogen, and oxygen in thorium. Metallurgical Society of the American Institute of Mining Engineers Transactions 236: 1311-1315. 1966.

34. Mordike, B. L. and Haasen, P. The influence of temperature and strain rate on the flow stress of alpha iron single crystals. Philosophical Magazine 7: 459-474. 1962.

35. Haasen, Peter. Plastic deformation of nickel single cyrstals at low temperature. Philosophical Magazine 3: 384-418. 1958.

36. Dieter, G. E. Mechanical metallurgy. 1st ed. New York, N.Y., McGraw-Hill Book Co., Inc. 1961.

37. Perry, C. C. The strain gage primer. 2nd ed. New York, N.Y., McGraw-Hill Book Company. 1961.

38. Budd Company. Instruments Division. Installation instructions for Tatnall 101 series epoxy back strain gages using epoxy adhesives: IB-6102, instruction manual. Phoenixville, Pa., author. 1965.

39. Armstrong, P. E., Carlson, O. N., and Smith, J. F. Elastic constants of thorium single crystals in the range 77-400°K. Journal of Applied Physics 30: 36-41. 1959.

40. Taylor, G. I. Plastic strain in metals. Institute of Metals Journal 62: 307-324. 1938.

41. Peterson, D. T. Diffusion of carbon in thorium. American Society for Metals Transactions 53: 765-773. 1961.

42. Smith, M. D. and Honeycombe, D. W. K. The effect of oxygen, carbon, and nitrogen on the properties of sintered thorium. Journal of Nuclear Materials 1: 345-355. 1959.

43. Peterson, D. T., Page, D. F., Rump, R. B., and Finnemore, D. K. Resistivity of very pure thorium and thorium-rare earth alloys. [To be published in Physical Review ca. 1967.]

44. Mott, N. F. and Jones, H. The theory of the properties of metals and alloys. First published 1936 by Clarendon Press, Oxford, England. Reprinted New York, N.Y., Dover Publications, Inc. 1958.

45. Friedel, J. On amplitude dependent internal friction. In National Physical Laboratory Symposium No. 15: 409-427. London, England, Her Majesty's Stationery Office. 1963.

46. Cottrell, A. H. Effect of solute atoms on the behavior of dislocations. In Report on a Conference on the Strength of Solids. pp. 30-35. London, England, Physical Society of London. 1948.

47. Bilby, R. A. On the interactions of dislocations and solute atoms. Physical Society of London Proceedings A63: 191-200. 1950.

48. Nabarro, F. R. N. The mechanical properties of metallic solid solutions. Physical Society of London Proceedings 58: 667-676. 1946.

49. Eshelby, J. D. Distortion of a crystal by point imperfections. Journal of Applied Physics 25: 255-261. 1954.

50. Fleischer, R. L. Solution hardening by tetragonal distortions: application to irradiation hardening in F.C.C. crystals. Acta Metallurgica 10: 835-842. 1962.

51. Fleischer, R. L. Solution hardening. Acta Metallurgica 9: 996-1000. 1961.

52. Kubaschewski, O. and Evans, E. LL. 3rd ed. Metallurgical thermodynamics. New York, N.Y., Pergamon Press. 1958.

53. Aronson, S. Thermodynamic properties of thorium carbides from measurements on solid E.M.F. cells. In Waber, J. T. and Chiotti, P., eds. Nuclear metallurgy. Compounds of interest in nuclear reactor technology. Volume 10. The Metallurgical Society of the American Institute of Mining Engineers. 1964.

54. Jost, W. Diffusion in solids, liquids, gases. New York, N.Y., Academic Press. 1952.

55. Rundle, R. E. A new interpretation of interstitial compounds: metallic carbides, nitrides, and oxides of composition MX. Acta Crystallographica 1: 180-187. 1948.

56. Wynnblatt, P. and Dorn, J. E. Dislocation mechanisms for plastic flow in an iron-manganese alloy at low temperature. Metallurgical Society of American Institute of Mining Engineers Transactions 236: 1451-1456. 1966.

57. Christ, B. W., Smith, G. V., and Burton, M. S. The influence of grain boundaries and veining subgrain boundaries on the yield phenomenon in zone-refined iron. Metallurgical Society of the American Institute for Mining Engineers Transactions 236: 9-13. 1966.

58. Adair, A. M., Hook, R. E., and McGaughey, R. L. The effect of thermal history on the yield behavior of iron. Metallurgical Society of the American Institute for Mining Engineers Transactions 236: 174-178. 1966.

59. Hahn, G. T. A model for yielding with special reference to the yield point phenomena of iron and related BCC metals. Acta Metallurgica 10: 727-738. 1963.

60. Van Torne, L. I. and Thomas, G. Yielding and plastic flow of niobium. Acta Metallurgica 11: 881-898. 1963.

61. Petch, N. J. The upper yield stress of polycrystalline iron. Acta Metallurgica 12: 59-65. 1964.

ACKNOWLEDGEMENTS

The author would like to express his appreciation to Mr. Lester Reed for his assistance in the preparation of samples and to Mr. Harlan Baker for his help and advice in the metallographic portions of the study. The author is particularly indebted to Dr. David Peterson for his encouragement, guidance, and patience throughout the course of the research.

APPENDIX

One must now relate the tensile stress externally applied to a polycrystal to the shear stress actually operating on active slip planes within individual grains. This problem has been studied by a number of investigators over a period of years. Cottrell (9) has summarized their work and his account will be briefly outlined. The original interest was in calculating the tensile yield strength of a polycrystal from the critical shear stress of a single crystal by use of an expression of the form

$$\sigma_o = m\tau_c$$

where σ_o is the yield strength of the polycrystal, τ_c is the critical shear strength of the single crystal, and m is the Schmidt factor for the most favorably oriented slip system in the grain. The maximum value for m is $\frac{1}{2}$, but the mean value, $\bar{m}$, obtained by integrating over all orientations of a face centered cubic polycrystal is 1/2.238. Through the assumption that all grains are equally strained, the idea was extended to relate the above relation over the entire stress strain curve. Taylor (40) was able to relate polycrystal aluminum stress strain curves with the corresponding single crystal curves with the expression

$$\sigma = \bar{m}\tau$$

where σ is the polycrystal tensile flow stress, τ is the single crystal resolved flow stress, and $\bar{m}$ is 3.1. The discrepancy between the observed factor 3.1 and the 2.238 value obtained on a strictly geometric basis was explained by the fact that grains in real metals are acted on by their neighbors. In this work the factor 1/3.1 was used to calculate the mean shear from tensile flow stress. This choice affects the values reported for τ^*, the effective shear stress, v^*, the activation volume, and dt/dC, the rate of strengthening.